Control Analysis of Active Dynamic Filtering Systems for Electrical Power Application

Max Rosenbäck

Frida Salehi

LUND UNIVERSITY

Department of Automatic Control

MSc Thesis
TFRT-6234
ISSN 0280-5316

Department of Automatic Control
Lund University
Box 118
SE-221 00 LUND
Sweden

Printed in Sweden by Tryckeriet i E-huset
Lund 2024

Abstract

This thesis investigates the behaviour of an active dynamic filtering (ADF) system connected to an unknown electrical grid and suggests how to use control theory to reach desired requirements. The ADF system, which is based on a product by Comsys AB, consists of a PI controller and a low pass filter.

The main part of this work was focused on developing methods for system identification by finding transfer functions between available signals utilising a grey box model approach. Different validation techniques were applied to gain trust in the model as well as the estimated transfer functions. By reworking the model and by using the estimated transfer functions, the electrical circuit could be reformulated as a block diagram to facilitate the use of standard control analysis. Methods of tuning the PI controller parameters to reach a certain bandwidth while keeping stable margins were presented. It was concluded that the resonances in the open loop transfer function had to be counteracted. Therefore, filter designs to compensate for this behaviour were also investigated and presented. Finally, a number of future developments were presented.

In conclusion, the method of estimating the transfer functions, yielding the system identification, is shown to be sufficient. Thus, the system behaviour can be understood and can be altered to achieve different requirements through control parameter tuning and filters. Future research could expand this work by applying this workflow on more realistic systems.

Key Words: System identification, PI controller, Electrical grid, Notch filter, Automatic control, Grey Box, Simulink

Acknowledgements

We would like to thank Nils Lundström, our supervisor at Comsys AB, for the opportunity to do this project as our Master's thesis and for your guidance and enthusiasm. Furthermore, we would like to thank our supervisor at the Department of Automatic Control, Lund University, Richard Pates for all the discussions we have had during our meetings and your invaluable help throughout this entire project. We are sincerely thankful and this project would not have been possible without either of you.

Abbreviations

AC Alternating current

ADF Active dynamic filtering

CES Combined estimated system

DC Direct current

I/O Input signal to output signal

L grid Inductive grid

LCL grid Inductive-capacitive-inductive grid

LHP Left half plane

MIMO Multiple input multiple output

NRMSE Normalised root mean square error

RHP Right half plane

SISO Single input single output

Contents

1

Introduction

This report comprises the thesis work carried out at Comsys AB in Lund, in close cooperation with the Department of Automatic Control at LTH, conducted between January and May 2024.

1.1 Background

A traditional electrical power grid has previously been composed of large stable producers and small reliable consumers. The grid was easily plannable and consumption grew at a predictable rate. This picture of the grid has been changing over the last decade into a two-way power flow system. Instead of having conventional consumers, now households have become producers themselves through, for example, domestic solar power. Some consumers now use the grid mainly to balance their own power generation and as a backup supplier when their own production is unavailable. [Henderson et al., 2017]

The major sources of production have also undergone a change from plannable fuels such as fossil and nuclear to an increasing amount of renewable energy sources instead. This change continuously creates a certain unreliability in the grid since these forms of production are dependent on appropriate conditions of nature. [Henderson et al., 2017]

Large consumers, such as industry, also put strains on the grid. The heavy processes create disturbances as well as vulnerability to different downgrades in the power quality. Such downgrades appear as different electrical disturbances such as transients, harmonics, flicker and oscillations. [Comsys AB, 2024a]

Especially harmonics can be harmful for an electrical system and these are in many cases created by the machinery of today. In a conventional alternating current system, the voltage varies at a frequency of 50 or 60 Hz called the grid frequency. The

increasing amount of pulse controlled devices and equipment creates nonlinear currents in the system, which gives rise to voltage disturbances creating a relatively complex wave shape. The switching employed for the pulse control also adds harmonics of the grid frequency. These harmonics can be detrimental to machinery and create heat losses, overheated cables and damage to sensitive equipment. [Linjengren, 2011]

Comsys and Active Dynamic Filtering

Comsys AB was founded 2001 in Lund, Sweden, and has since then grown into a globally present cleantech company focusing on electrical power systems. Comsys' main innovation is their active dynamic filtering (ADF) system which has resulted in a number of products installed in many fields such as industry and the naval sector. [Comsys AB, 2024b] The ADF method, used in products of Comsys, starts with a measurement of electrical voltage at the electrical system of interest in order to derive a value of the current. This current is then compared to a reference current, creating a current error vector. From the error vector an upper and a lower threshold value is calculated. A system of switches is then used to feed current from a direct current source to the electrical system depending on the current error. This method compensates the current consumption of the loads at frequencies that would not exist if the load was purely resistive and, in that way, counteracts the disturbances and issues created by modern non resistive equipment.

The method is realised using an active filter comprised of a DC source, a system of switches, a DC current conductor as well as the control unit that uses a voltage measuring unit, a calculating unit, and a system of switches, calculating and creating the compensation current. To remove frequencies other than the fundamental frequency from the filter's system of switches, a capacitive leg from the DC current conductor to earth is also added. [Linjengren, 2011]

A deeper understanding of Comsys' products and the ADF method is not needed for this thesis. The set limitations on the problem formulations and the simplified simulation environment used for the experiments allow for this more general comprehension of the product. The expectation from Comsys is to find a structured workflow based on known theory instead of manual tuning, using their current product set up. It is also a wish to investigate whether the control could be improved using other signals than the currently measured and controlled current I_{adf}.

1.2 Problem Formulation

This thesis aims to investigate solutions to the following problems:

- Find a method for system identification on a model, representing Comsys'

product connected to an unknown grid, by identifying frequency behaviour and all relationships between signals through estimations on data from simulations.

- Investigate how different control designs affect the bandwidth and stability margins of the system, focusing on the present PI controller of the product, but also suggesting how new methods can be incorporated to obtain wanted system behaviour.

Solutions to these problems would be the first initiatives in a larger project to create an automatic solution which changes parameters of the controller depending on a changing grid.

1.3 Resources

Simulink Model

The necessary resources for this thesis were provided by Comsys, which included a simplified model of a controller, a low pass filter and an electrical grid. The model was built in Matlab Simulink and it connects a mathematical signal from a controller to an electrical circuit. A detailed illustration of the Simulink model can be seen in Appendix 8.2, but a simplified version is provided below in Figure 1.1 followed by a short description.

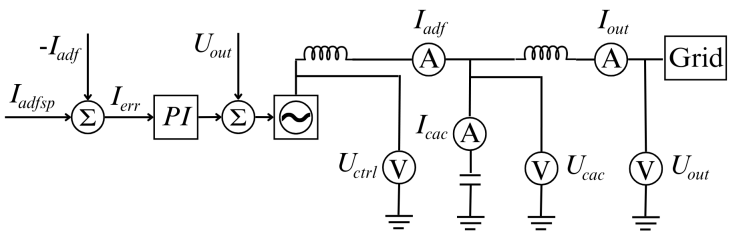

Figure 1.1 Simplified version of the Simulink model.

In Figure 1.1, the mathematical signals and measurements are shown with arrows, while the electrical circuits are straight lines. Inductors, capacitors and earth are represented by their conventional symbols. All currents and voltages used in this thesis are shown next to the corresponding ammeter or voltmeter. However, the only signals that are actually measurable in the Simulink model are I_{adfsp}, I_{adf}, U_{ctrl}, U_{out}, and I_{out}, of which the last one is not measurable in real life.

The input of the system is a sinusoidal current reference signal I_{adfsp} (active dynamic filter set point), produced by a sine wave generator, with an amplitude of 1 Ampere and a frequency that is determined by the objective of each experiment. Negative feedback of the current I_{adf} (active dynamic filter) is then added to the set point creating the signal I_{err} (error) that is fed into the controller.

The controller is a simple PI controller with one proportional term and one integral term. The resulting control signal is added to a positive feedback of U_{out}, the grid voltage. Through a controlled voltage source the signal is turned into a control voltage, U_{ctrl}, on the electrical circuit. Connected in the electrical circuit is the low pass filter, consisting of one inductor connected to a parallel leg with a capacitor connected to earth and an arm with one inductor connected to the outside grid. From the arm of the filter connected to the controller measurements of the current I_{adf} is extracted and from the point after the filter the voltage U_{out} is measured. Continuing in the electrical circuit, the grid is either constructed as two inductive loads in series or a similar setup but with a capacitive leg in the middle of the two inductors (not shown in the simplified Figure 1.1). The power source of the grid is an ideal DC voltage source with constant voltage.

All relevant signals are measured with either current measurement blocks or voltage measurement blocks connected to scopes that track the signals. These scopes are set to log the last $\frac{1}{base\_freq \cdot t\_sim}$ data points which in all presented experiments are 20,000 data points.

1.4 Limitations in Thesis Scope

To create a reasonable approach of the problem a number of limitations were added to the problem formulation.

All of the data, utilised in the method and conclusions of this thesis, was created in the Simulink model described in section 1.3. The data was sampled with a sample frequency of 10^6 Hz and the data points were produced from a change of frequency in the input signal with an increase of 100 Hz from 100 Hz to 6000 Hz.

The electrical grids modelled in Simulink were exclusively handling direct current in a single-phase system and not a three-phase AC grid that forms the majority of real-life implementations. In the thesis, it is also assumed that the grid consists of either purely inductive loads in series or inductive loads and capacitive loads in parallel connection. Furthermore, the model is not taking into account the discrete switching of voltages used in Comsys' actual product and instead it is modelled as a continuous system.

1.5 Contribution to the Development of Knowledge

This Master's thesis is expected to contribute to the development of knowledge. As a result of the global electrification and the transition to renewable energy there will be an increasing demand for knowledge in this area. As a consequence, this thesis is valuable from an environmental transition point of view. Furthermore, it will contribute to the knowledge of integrating automatic control on an electrical grid. Since this thesis is performed at Comsys AB it will contribute to their overall aim of creating solutions to challenges emerging in the power industry.

1.6 Specification of Contributions from the Authors

This Master's thesis was produced by the two authors, Max Rosenbäck and Frida Salehi, in close cooperation. All simulations and development of methods were done by both authors, and the amount of breakthrough ideas were shared evenly.

In the report, the different sections were initially divided between the authors, but the final version was read through and revised by both authors. Thus, the final report is a completely collaborative result.

More specifically, most of Chapter 1 was initially handled by Max, while Chapter 2 was written by Frida. However, the methods, the results and the discussions were constructed through an ongoing dialogue between the authors. Thus, an equal amount of contribution was made to the rest of the chapters.

2

Theory

2.1 System Identification and Mathematical Models

Systems and Models

Control system analysis relies on mathematical models of a system. Thus, it is of great value to describe a system with an accurate model before applying control methods. [Ljung et al., 2015]

Systems can be described as mathematical models by defining the relationships between quantities in the system, for instance the relationship between currents in a circuit. There are different approaches to building a model, two of which are referred to as physical modelling and identification. Physical modeling uses laws of nature, for example Kirchhoff's law in a circuit to construct a life-like model of a known system. On the contrary, identification relies on observations of a system, such as measurements, to determine a model. When the system is unknown, the latter is the required approach out of the previously described modelling techniques. [Ljung et al., 2021]

Black Box Model. In order to model a completely unknown process mathematically, a black box model can be applied. The assumption that the system is a linear time-invariant (LTI) system makes it possible to do the following analysis. By studying solely the input and the output signal from the process, a relation between these signals can be acquired without knowing any of the physical dynamics of the process itself, for example by changing the frequency of the input signal and study the frequency response of the process. These relations between signals can form a basis of the model. A black box can be used to describe an entire system as a model or solely to describe a component in a larger system. [Ljung et al., 2021]

Grey Box Model. Another approach of mathematical modelling of a system is called grey box modelling. The assumption that the system is LTI makes it possible to do the following analysis. By knowing some of the dynamics of a system a more accurate description of a model can be obtained. A model can be derived from the

physical laws of a system and the grey box model is mainly used to approximate the unknown parameters. Instead of using a black box approach, where both the order of the system and the unique parameters have to be estimated, the number of zeros and poles a system is expected to have can be theoretically calculated and a model can be fitted to the data by only changing the parameters. This limits the number of models that has to be iterated and it saves both time and computational power. [Ljung et al., 2021]

Verification of a Model

It is necessary to verify that the model is functional for the purpose it is going to be used for. Therefore, there are a few factors that can be taken into account when validating the model. The input signal to output signal behaviour of the estimated model should replicate the behaviour of the signals in the original system. Moreover, the complexity of the model should be a reasonably accurate estimation of reality. If possible, this could be confirmed by comparisons to theoretical calculations of the system. [Ljung et al., 2021]

There are several different ways to verify the model and the method of estimation, one of which is using validation data. By testing the model on a new data set, independent of the data that was used to approximate the model, the consistency of the model can be verified. [Ljung et al., 2021]

Furthermore, gap metric is a distance metric that could be used for verification. The metric measures the distance between two systems with regard to the dynamic response. It can be interpreted as how well one system approximates another, and thus, the precision of an estimation compared to the actual transfer function can be measured through this metric. Gap metric takes values in the range 0 to 1, where a small value indicates that the two systems are similar to the extent that they can be controlled by the same controller. [Montandon Neto and Cunha, 2019]

System Identification Through Frequency Response Analysis

A system can be identified by its behaviour at different frequencies. Therefore, systems can be analysed by studying the signal behaviour at different input signal frequencies. By measuring a system over a range of frequencies and calculating the Fourier transform of the time domain data a frequency response can be constructed. For the case of a discrete set of data, the discrete Fourier transform can be used, transforming $y(k)$ to $Y(f) = T\sum_{k=1}^{N} y(kT)e^{-jfkT}$, where T is the sampling interval.

By making the assumption that the system is LTI, the relationship between input, $U(jf)$, and output, $Y(jf)$, can be described as $G(jf) = \frac{Y(jf)}{U(jf)}$. This estimation is especially accurate if all input signals are sinusoidal. [Ljung et al., 2021]

2.2 Electrical Principles in a Circuit

Each node in an electrical circuit follows Kirchhoff's current law, which states that the sum of all currents in the node is equal to zero.

$$\sum_{n=1}^{N} i_n = 0 \tag{2.1}$$

Throughout the circuit, each loop also follows Kirchhoff's voltage law, where the sum of all directed voltage differences around a closed loop is equal to zero.

$$\sum_{n=1}^{N} V_n = 0 \tag{2.2}$$

Finally, Ohm's law states that the voltage difference over an impedance is equal to the impedance multiplied with the current flowing through it.

$$\Delta V = i \cdot \Omega \tag{2.3}$$

[Alfredsson and Rajput, 2009]

A passive system is a system that does not contain any current sources, voltage sources or other active components. Passive components include for instance resistors, inductors and capacitors. These components only store, release or dissipate and they do not generate power. [Alfredsson and Rajput, 2009]

2.3 Control Theory

Stability and Robustness

Consider a simple feedback connection of a SISO process, $G(s)$, and a controller, $K(s)$. From this follows that $G_{cl}(s) = \frac{G(s) \cdot K(s)}{1 + G(s) \cdot K(s)}$ is the closed loop transfer function. A criterion that guarantees input-output stability of a system is that $G_{cl}(s)$ is Hurwitz, which means that all poles of $G(s)$ exist in the left half plane. Furthermore, the Nyquist criterion states that the sum of the number of right half-plane poles and the number of clockwise encirclements of -1 is equivalent to the number of unstable poles of the closed loop system $G_{cl}(s)$. [Hespanha, 2009]

Both the sensitivity function ($S(s) = \frac{1}{1+G(s)\cdot K(s)}$) and the complementary sensitivity function ($T(s) = \frac{G(s)\cdot K(s)}{1+G(s)\cdot K(s)}$) have to be stable in order to have an internally stable closed loop system. With regard to having a satisfactory disturbance rejection at low frequencies, S should be small. Furthermore, at low frequencies T should be close to 1 since it indicates effective reference tracking. At high frequencies, a small T indicates noise rejection. [Hespanha, 2009] Limits on gain and phase margins can be turned into a constraint on the maximum sensitivity. With a maximum sensitivity below 2, stable margins are guaranteed. [Åström, 2019]

Tuning PI Controller Parameters

For a process, $G(jf)$, controller, $K(jf)$, the open loop transfer function, $L(jf)$, and closed loop transfer function, $T(jf)$, are defined as the following:

$$L(jf) = G(jf)K(jf) \text{ and } T(jf) = \frac{L(jf)}{1+L(jf)}$$

By approximating the phase of $L(jf)$ to -90°, the following is obtained.

$$L(jf) = -j \Rightarrow \mid L(jf) \mid = 1 \Rightarrow \mid T(jf) \mid = \frac{\mid L(jf) \mid}{\mid 1+L(jf) \mid} = \frac{1}{\sqrt{2}} \tag{2.4}$$

The definition of bandwidth f_b is the maximum frequency where $\mid T(jf) \mid > \frac{1}{\sqrt{2}}$. The cross-over frequency is defined as $\mid L(jf_c) \mid = 1$. Thus, from equation 2.4 the closed loop bandwidth can be approximated to the open loop cross-over frequency, $f_b \approx f_c$ such that $\mid L(jf_c) \mid = 1$. [Frazzoli, 2017]

A standard PI controller, $K(s) = \frac{K_i+K_p s}{s}$ has the following Bode diagram:

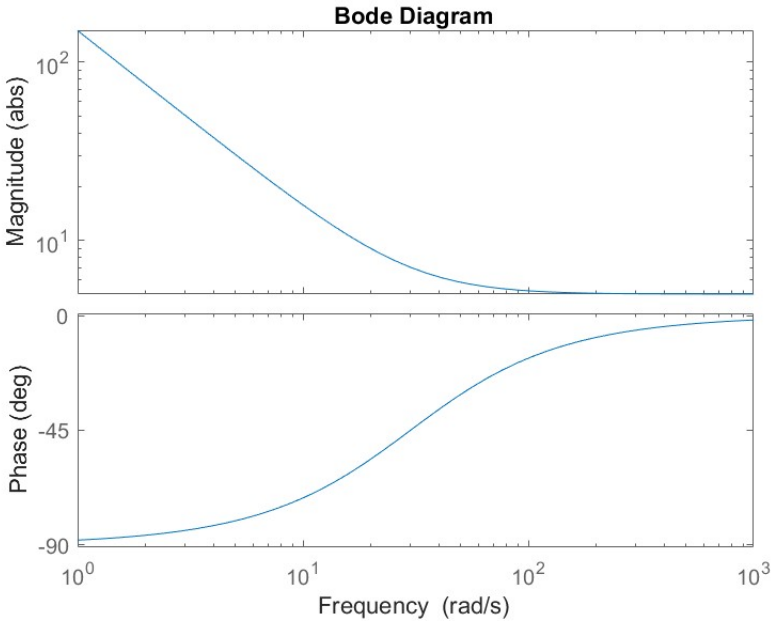

Figure 2.1 Bode diagram of PI controller with Kp=5 and Ki=150.

The PI controller starts with a slope of -1 in amplitude and a phase of $-90°$ because of the pole in 0. The PI controller has a LHP zero as well, which can be calculated from $K_i + K_p z = 0 \Rightarrow z = -\frac{K_i}{K_p}$ and this will result in a slope increase of 1 and a phase increase of $90°$. From the magnitude plot a corner can be identified at a certain corner frequency, where the slope of the magnitude goes from -1 to tending to 0. The corner frequency is at $\frac{K_i}{K_p}$ because of the LHP zero. Depending on the wanted bandwidth, f_b of the closed loop system, the parameters K_i and K_p can be varied. [Hägglund, 2009]

Filters

Lag Compensator. A lag compensator can be introduced to a system in order to increase the gain for low frequencies. The transfer function of a lag compensator can be written as the following:

$$G_K(s) = \frac{s+a}{s+a/M} \tag{2.5}$$

Rules of thumb for designs of the lag compensator is to choose M depending on the desired decrease of the stationary error and a as the frequency where the gain breaks down from M to 1. To avoid affecting the phase margin, a should be chosen at a distance from the cross-over frequency and a good rule is $a = 0.1 \cdot f_c$.

[Hägglund, 2009]

Lead Compensator. A lead compensator increases the phase of the system, which is usually suitable to raise the phase margin at the cross-over frequency. The compensator is designed as following:

$$G_K(s) = K_K N \frac{s+b}{s+bN} \tag{2.6}$$

The rule of thumb of designing a lead compensator is to proceed from a desired cross-over frequency, f_c, and phase margin, φ_m.The parameter N should be decided from the desired φ_m because it determines the magnitude peak of the phase rise. In order to place the phase rise at the cross-over frequency, b should be chosen as $b = \frac{f_c}{\sqrt{N}}$. Finally, K_K is chosen such that the gain of the desired cross-over frequency is 1.

[Hägglund, 2009]

Notch Filter. In order to reject frequencies within a certain frequency range, f_0 to f_1, band stop filters can be used.

$$H(f) = \begin{cases} 1 \; 0 \leq f \leq f_0 \\ 0 \; f_0 \leq f \leq f_1 \\ 1 \; f_1 \leq f \end{cases} \tag{2.7}$$

If the band of which the wanted frequencies to reject is narrow, with a width ε, the band stop filter is called a notch filter.

$$H(f) = \begin{cases} 1 \; 0 \leq f \leq f_N - \varepsilon \\ 0 \; f_N - \varepsilon \leq f \leq f_N + \varepsilon \\ 1 \; f_N + \varepsilon \leq f \end{cases} \tag{2.8}$$

The notch filter in the Laplace domain can be written as the following:

$$H(s) = \frac{s^2 + f_N^2}{s^2 + \sqrt{2} f_N s + f_N^2} \tag{2.9}$$

The variable f_N is the desired frequency of the notch. To the expression above, more terms can be added for more specific designs of notch filters.

[Ducard, 2018]

3

Methodology

The approach to answering the problem formulations of this thesis consisted of both system identification and control design focused on the ADF system connected to an unknown grid. This approach was further divided into four major parts. First of all, data of the system was acquired through simulations in Simulink. This data was then utilised to find a model and estimation of the system behaviour. To verify the results of the estimations, different methods of validation were performed. Once a verified and accurate model of the system had been estimated, control analysis tools were used to design a controller to reach desired system behaviours.

3.1 Simulations

The first step in identifying the system and estimating a model was acquiring the data through simulations. These were run in a Simulink model (see figure in Appendix 8.2). This Simulink model was provided at the start of the thesis and is described in further detail in section 1.3: *Simulink Model*. The grid parameters used in the simulations are shown in Appendix 8.1 and will hereon be referred to as standard grid parameters.

The simulations were run over a time period of 0.05 seconds to remove transient behaviour. The sinusoid input signal was held at a steady frequency while voltage and current meters gave measurements at different points in the electrical system. The last 20,000 data points of the accessible signals were saved in data structures. With a sample frequency of 10^6 Hz this data corresponded to the last 0.02 seconds of the simulation. The signals that were measured and stored in the structures were the input signal I_{adfsp}, the current that is of interest from a control perspective I_{adf}, the current leaving the filter I_{out}, the voltage at the point between filter and grid U_{out} and the voltage generated from the source connected to the control system U_{ctrl}.

To be able to identify the system through frequency response, a larger set of frequency data was collected. This was achieved by increasing the frequency, f, of the input signal, I_{adfsp}=$sin(2\pi f)$, by 100 Hz from 100 Hz to 6000 Hz and running a separate simulation for each of these frequencies. The result was a large structure with 20,000 values for 60 different frequencies for each of the measurable signals.

3.2 System Identification

The system identification consisted of two parts, first finding a model representing the system and then estimating the various transfer functions in the model through calculations conducted in Matlab. To verify the success of the estimations, three different methods were used to calculate a transfer function from input signal to output signal and these were later used for cross verification to make certain the validity of the model and the method of estimation. The different methods of obtaining transfer functions were based on finding them through:

1. a direct relation between input signal and output signal estimated from data acquired from simulations.

2. a system established from theoretically calculated transfer functions based on known parameters and electrical principles.

3. a system based on a grey box model with transfer functions estimated from data acquired from simulations.

Modelling Using Black Box and Grey Box Approach

To understand how the simulation data was connected to the signals and how the system was comprised, a possible mathematical model of the system had to be produced. Since it was assumed that the available information of the system was limited, a grey box approach was employed. The given Simulink model and the character of the impedances could be used to have a basic understanding of the system behaviour. However, the values of the impedances were assumed to be unknown. In order to analyse and apply control theory on the system in later stages it was also seen as preferable that the controller was separated from the system.

Firstly, the system, except the controller, was treated completely as a black box and with this approach the system could be rewritten on the form shown in Figure 3.1.

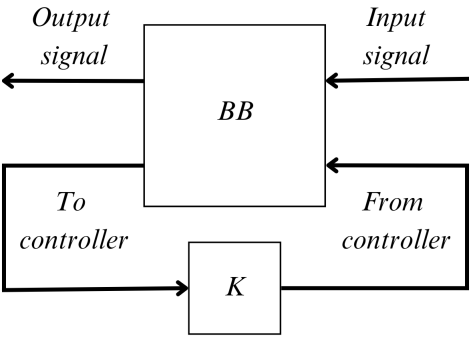

Figure 3.1 Initial black box model.

This basic modelling approach depended on identifying which signals were the relevant output signals, input signals and signals sent to and from the controller. In the simplified figure (see Figure 1.1), it can be observed that the only signal sent into the system is I_{adfsp}. The relevant signal from a control perspective is I_{adf} and the signal sent from the controller is U_{ctrl}. Thus, three out of four signals were easily identifiable. However, U_{ctrl} contains both the difference between I_{adf} and I_{adfsp}, (I_{err}), which is sent through the PI controller and the added signal U_{out}. From an electrical perspective, this corresponds to the grid voltage being added to the control voltage. To facilitate this behaviour, the black box of the model was expanded into a matrix.

By identifying these input and output signals, a more detailed description of the model was obtained. The black box was treated as a MIMO system (see Figure 3.2).

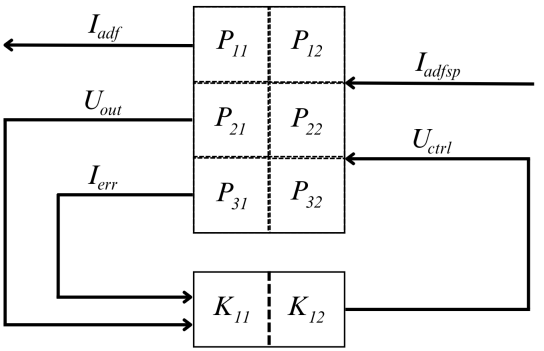

Figure 3.2 Black box model with expected relationships between signals P_{11}-P_{32}.

This model corresponds to the following matrix equation:

$$\begin{pmatrix} I_{adf} \\ U_{out} \\ I_{err} \end{pmatrix} = \begin{pmatrix} P_{11} & P_{12} \\ P_{21} & P_{22} \\ P_{31} & P_{32} \end{pmatrix} \begin{pmatrix} I_{adfsp} \\ U_{ctrl} \end{pmatrix}, \; U_{ctrl} = \begin{pmatrix} K_{11} & K_{12} \end{pmatrix} \begin{pmatrix} U_{out} \\ I_{err} \end{pmatrix} \tag{3.1}$$

This mathematical model contains the relationships between all relevant signals. From this point each transfer function (P_{11}-P_{32}) could be estimated or, if the impedances of the system were known, identified by theoretical calculations, and then combined into a model of the entire system.

Identifying Relationships Between Signals

Since all parameters of the Simulink model were known, theoretical calculations could be used to understand the exact relationships between the voltages and the currents. In order to further identify the exact relations between the signals in the system, a block diagram (see Figure 3.3) of the electrical circuit excluding the controller could be constructed.

This block diagram was obtained by using the impedances as blocks that transformed the signals. The feedback loops were used to construct current division and voltage drops following Kirchhoff's laws described in section 2.2. The impedance of the grid, Z_g, could easily be calculated for both an L and an LCL grid. The values and the character of the impedances used in the block diagram can be seen in table 3.1. Noticeably, all signals shown in the simplified figure (see Figure 1.1) are present in this block diagram representation of the system.

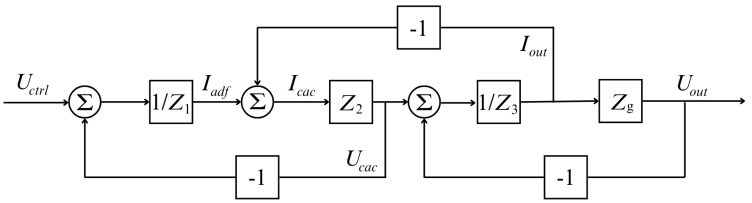

Figure 3.3 Block diagram of the system after the controller.

Table 3.1 Table consisting of the impedances used in block diagram in Figure 3.3.

Impedance	Value	Position
Z_1	R+L1·s	Left inductive arm in filter
Z_2	R+1/(Cac·s)	Capacitive leg in filter
Z_3	R+L2·s	Right inductive arm in filter
Z_4	R+Lg2·s	Left inductive arm of grid
Z_5	R+Lg1·s	Right inductive arm of grid
Z_6	R+1/(Cg1·s)	Capacitive leg in grid (LCL grid)
Z_g	Z_4+Z_5	Combined impedance of grid (L grid)
Z_g	Z_4+$Z_5 \cdot Z_6/(Z_5+Z_6)$	Combined impedance of grid (LCL grid)

From this block diagram a set of equations could be constructed from which the transfer functions between each signal could be calculated. Each relation between signals was given a name. The following calculations were made:

$$U_{out} = \frac{Z_g}{Z_3}(U_{cac} - U_{out}) \;\Rightarrow\; U_{out} = \frac{Z_g}{Z_3 + Z_g}U_{cac} = J \cdot U_{cac} \tag{3.2}$$

$$I_{out} = \frac{1}{Z_3}(U_{cac} - J \cdot U_{cac}) \;\Rightarrow\; I_{out} = \frac{1-J}{Z_3}U_{cac} = L \cdot U_{cac} \tag{3.3}$$

$$U_{cac} = Z_2(I_{adf} - L \cdot U_{cac}) \;\Rightarrow\; U_{cac} = \frac{Z_2}{1 + Z_2 \cdot L}I_{adf} = M \cdot I_{adf} \tag{3.4}$$

$$I_{adf} = \frac{1}{Z_1} \cdot (U_{ctrl} - M \cdot I_{adf}) \;\Rightarrow\; I_{adf} = \frac{1}{Z_1 + M}U_{ctrl} = N \cdot U_{ctrl} \tag{3.5}$$

With the newly acquired transfer functions, a new block diagram of the system was obtained, see Figure 3.4.

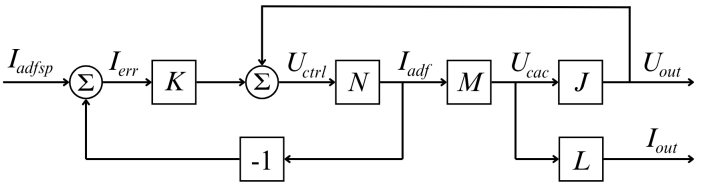

Figure 3.4 Block diagram of entire system with named transfer functions between each signal.

This resulted in the transfer functions necessary to identify all elements of the matrix of the mathematical model presented in Figure 3.2.

$$U_{out} = N \cdot U_{ctrl} \;\Rightarrow\; P_{12} = N$$

$$U_{out} = JMN \cdot U_{ctrl} \;\Rightarrow\; P_{22} = JMN$$

Looking at the relation between I_{adf} and I_{adfsp}, it can be seen that the whole correlation is already existent in U_{ctrl}. This resulted in $P_{11} = 0$ and the same reasoning gave $P_{21} = 0$ between U_{out} and I_{adfsp}.

Finally I_{err} is defined as:

$$I_{err} = I_{adfsp} - I_{adf} = I_{adfsp} - N \cdot U_{ctrl}$$

$$\Rightarrow P_{31} = 1 \; and \; P_{32} = -N$$

Thus, with this information the black box model could be rewritten as a grey box model 3.5. It should also be noted that the current I_{out} does not affect any other signal. Thus, it was not incorporated in further model representations.

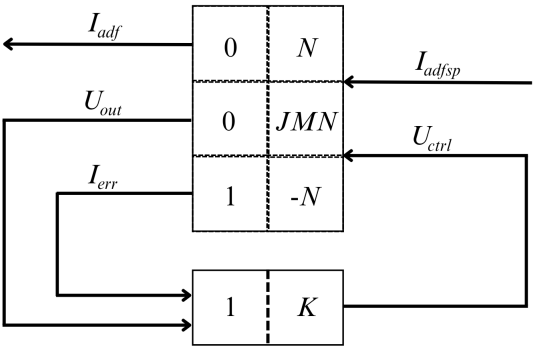

Figure 3.5 Grey box model with all elements identified.

This model corresponds to the following matrix equation:

$$\begin{pmatrix} I_{adf} \\ U_{out} \\ I_{err} \end{pmatrix} = \begin{pmatrix} 0 & N \\ 0 & JMN \\ 1 & -N \end{pmatrix} \begin{pmatrix} I_{adfsp} \\ U_{ctrl} \end{pmatrix}, \; U_{ctrl} = \begin{pmatrix} 1 & K \end{pmatrix} \begin{pmatrix} U_{out} \\ I_{err} \end{pmatrix} \tag{3.6}$$

Introducing New Signal for Controller Separation

The model constructed above was sufficient to find the relationship between each of the signals in the system and therefore, it was an important step to understand all system behaviours. However, in order to apply control theory on the system described as the grey box model it was more suitable to separate solely the PI controller from the rest of the system. This could be done by introducing a new signal, $U_{prime} = U_{ctrl} - U_{out}$. The following calculations were made to find the relationships between this new signal and the previous ones:

$$U_{out} = JMN \cdot U_{ctrl} \Rightarrow U_{prime} = U_{ctrl} - U_{out} = (1 - JMN) \cdot U_{ctrl} \Rightarrow U_{ctrl} = \frac{1}{1 - JMN} U_{prime} \tag{3.7}$$

$$I_{adf} = N \cdot U_{ctrl} \Rightarrow I_{adf} = \frac{N}{1 - JMN} U_{prime} \tag{3.8}$$

$$I_{err} = I_{adfsp} - I_{adf} = I_{adfsp} - N \cdot U_{ctrl} = I_{adfsp} - \frac{N}{1 - JMN} U_{prime} \tag{3.9}$$

Inserting these relationships into a new grey box model resulted in the following:

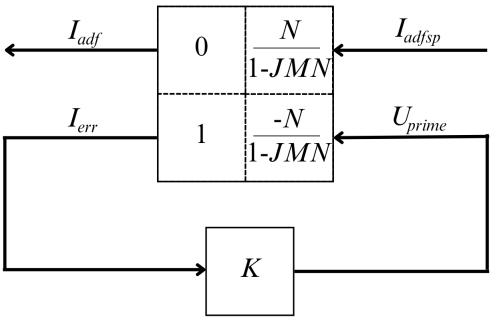

Figure 3.6 Grey box model with solely the PI controller separated and the introduced signal $U_{prime} = U_{ctrl} - U_{out}$.

With corresponding matrix equation:

$$\begin{pmatrix} I_{adf} \\ I_{err} \end{pmatrix} = \begin{pmatrix} 0 & \frac{N}{1-JMN} \\ 0 & \frac{-N}{1-JMN} \end{pmatrix} \begin{pmatrix} I_{adfsp} \\ U_{prime} \end{pmatrix}, \; U_{prime} = K \cdot I_{err} \tag{3.10}$$

This model could further be rewritten as a simple block diagram with a feedback loop with controller, $K = K_p + \frac{K_i}{s}$, and process, $G = \frac{N}{1-JMN}$.

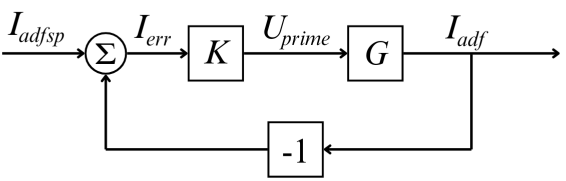

Figure 3.7 Block diagram with the introduced signal U_{prime}.

The resulting system with the use of the new signal U_{prime} presented the opportunity to analyse the open loop system as well as the closed loop system from a control perspective. It should be recognised that all the measurable signals presented in section 1.3, except I_{out}, still appear in the model, since U_{prime} is a combination of U_{ctrl} and U_{out}.

Estimation of Transfer Functions from Simulation Data

To convert the data acquired in section 3.1 to transfer functions that can be used in the model described above, a method of estimation was necessary. This method was constructed using some of Matlab's system identification and control tools and it will be described in short in the following section.

Converting the Data. To find a transfer function between two signals, the data structures of these signals, consisting of the 20,000 data points per frequency from the conducted simulations of 60 different frequencies, were collected. The discrete Fourier transform was used to convert the data from the time domain to the frequency domain. From the transformed data, the corresponding frequency of the input signal was extracted. By doing this for all frequencies an array of 60 data points, each a complex number, was acquired with a corresponding frequency. From each data point the amplitude, $A(jf)$, and the phase, $\phi(jf)$, could be obtained for each distinct frequency. In that way each data point could be written as the result of a function of frequency which is shown in equation 3.11.

$$y(jf) = A(jf) \cdot e^{(j \cdot \phi(jf))} \tag{3.11}$$

Estimating the Transfer Function. To estimate the transfer function between two signals, the relation between the two complex data sets were calculated pointwise. The result was a new array of 60 complex data points that corresponded to the transfer function between the two signals.

There were two different ways to continue with the estimation of the transfer function from these data points. If nothing is known about the structure of the transfer function, the Matlab function *tfest()* from the system identification toolbox could be used. The input to this function was an idfrd object (frequency response data object) consisting of the data points written on the form given in equation 3.11. The idfrd object is Matlab's way of connecting every element in the array of frequency responses (one for each data point) to the corresponding frequency. The function *tfest()* iterates different degrees of the numerator and the denominator, and estimates parameters in order to match the data points in the idfrd object as accurate as possible in a complete black box approach.

To use a grey box approach, the Matlab function *pem()*, from the system identification toolbox, could be used, given that the degree of the transfer function is already

known. Inputs to *pem()* are the data points of the transfer function (stored in an idfrd object) and the order of which the data should be fitted to. The function then applies numerical optimisation to minimise the cost function $\sum_{n=1}^{N} e^2(n)$, where e(n) is the prediction error.

In this thesis, the second way of estimation was used since the degree of the system could easily be calculated theoretically. The degree of the transfer functions is independent of the values of the grid parameters and thus, this can be used even when the values of the parameters are unknown.

The result of the method described in this section was a Matlab transfer function object that was best fitted to the data points through the chosen fitting method (*tfest()* or *pem()*).

Estimations of the Entire System. Firstly, the estimation method was tested on the grey box model in Figure 3.5. In this model both the transfer function named N and the transfer function named JMN had to be estimated. This was done through the estimation program described above. Transfer function N corresponds to the relation from U_{ctrl} to I_{adf} and JMN corresponds to the relation from U_{ctrl} to U_{out} and these were estimated using Matlab's function *pem()*, with the simulated data points. Importantly, the degree of the expected transfer functions had been received through the theoretical calculation and could be used in the estimation to obtain a more accurate result.

When these relations of the individual signals had resulted in estimated transfer functions, the full system was combined by placing the functions at the correct index of the matrix and then using Matlab's linear fractional transformation function, *lft()*, to connect the system to the controller. The full system is still described by the transfer function from signal I_{adfsp} to I_{adf}, but instead of just an estimated relation between these two signals, the system is now separated from the controller and connected again. This is hereon referred to as the combined estimated system (CES).

The calculations mentioned above, done through Matlab's *lft()*, could simply be done by hand as well. From equation 3.6 the following is obtained:

$$\begin{cases} I_{err} = \frac{(1-JMN)}{K} U_{ctrl} \\ I_{adfsp} = (\frac{1-JMN}{K} + N) U_{ctrl} \end{cases} \quad \Rightarrow I_{adf} = \frac{NK}{1-JMN+NK} I_{adfsp}$$

Thus, the transfer function of the entire system (I_{adfsp} *to* I_{adf}) is $\frac{NK}{1-JMN+NK}$ and it is the same transfer function that is obtained from Matlab's *lft()* command.

Estimations of the Process. Instead of estimating each relation by itself, the entire process G (see block diagram in Figure 3.7) could be estimated. When control analysis was applied on the system, it was the estimation of the process G that was used with the motivation that fewer estimations and calculations had to be done.

3.3 Model and Estimation Validation

To verify the choice of model, comparisons were made between the transfer function estimated from the direct relation between the input and output signal and the transfer function estimated of the entire system (CES). Validations were also made between the estimated transfer functions between the different signals and the theoretically calculated transfer functions with the same known parameters. By also changing the different parameters of the impedances and reworking the estimations over a range of values, the reliability of the model was tested.

Specifically, the normalised root mean square error between the data and the corresponding estimated transfer function was calculated for each tested configuration of the grid. The calculations were done using the Matlab function *compare()* and they followed equation 3.12.

$$NRMSE = 100\left(1 - \frac{\|y - \hat{y}\|}{\|y - \bar{y}\|}\right) \tag{3.12}$$

In the equation, y is the data points from the simulation, $\hat{y}$ is the corresponding value of the estimated model and $\bar{y}$ is the mean value of the data points from the simulations, resulting in an NRMSE value as a percentage.

To further validate the black box model and the workflow, this NRMSE value was calculated for a number of different grids. The changes subjected on the grid compared to the standard grid parameters (section 8.1 in Appendix) were either on the first inductor, Lg1, or the capacitor, Cg1, in the electrical grid.

Furthermore, validations of the transfer function of the process, G, were made between the one theoretically calculated and the one that was estimated through data from simulations. These comparisons were made using Matlab's *gapmetric()*.

In order to test the robustness, new simulations were run where noise was added to the voltage source (U_{ctrl}) using a band-limited white noise block in Simulink. The resulting data was used to estimate transfer functions of the system and *gapmetric()* was employed to analyse the impact of the noise on the result. The purpose of these simulations was to test to what extent the estimation methods described above could handle noise. The output of the band-limited white noise block was depen-

dent on a parameter called noise power, which was iterated with reasonable values, determined by observation of the output from the block.

3.4 Control Design

Tuning PI Controller for Bandwidth Requirement

With the estimated model calculated in previous sections, suitable parameters for the controller could now be investigated. Since the system was stable, the purpose of the controller was to enhance performance by securing a certain bandwidth. This was done by following the theory of section 2.3: *Tuning PI Controller Parameters*.

The frequency response of the process, G, will be changed when multiplied with the PI controller. The presence of an integrator will result in a corner frequency as seen in section 2.3. Before the corner frequency the magnitude of the frequency response will be multiplied by $\frac{K_i}{s} + K_p$. After the corner frequency the contribution of K_i will rapidly decrease until the magnitude of the frequency response is only multiplied by K_p. These changes can be directly seen in the Bode plots by a shift of the plot in magnitude direction.

Thus, if a requirement is set on the bandwidth of the system at a frequency named f_b the PI controller parameters can be tuned such that this requirement is met. Assuming that the phase margin of the closed loop system is close to 90° at the crossover frequency (deduced from observations of the Bode plot) the gain of the system should be changed adequately so that $\mid \mathbb{L}(jf_b) \mid = 1$ (deduced from the simplicity of the model before the wanted crossover frequency). A more detailed explanation of this can be found in section 2.3: *Tuning PI Controller Parameters*. The relation described in equation 2.4 further provides $\mid 1 + \mathbb{L}(jf_b) \mid = \sqrt{2}$ and $\mid T(jf_b) \mid \approx \frac{1}{\sqrt{2}}$ which in turn defines the bandwidth of the system. By calculating the gain of the open loop system without controller $\mid G(jf_b) \mid$ at f_b and then choosing K_p as $\frac{1}{|G(jf_b)|}$, a bandwidth of the closed loop system close to the requirement will be acquired.

Since integral behaviour is desirable for the tracking of reference signals, $\frac{K_i}{s}$ has to be added. In order to get a reasonable phase margin, K_i was chosen such that $K_i = 0.1 \cdot f_b \cdot K_p$. The PI controller will contribute with a phase of -90°. Thus by choosing $K_i = 0.1 \cdot f_b \cdot K_p$, the LHP zero will be at the frequency $s = \frac{K_i}{K_p} = \frac{0.1 \cdot f_b \cdot K_p}{K_p} = 0.1 f_b$. This is a frequency well below the wanted bandwidth and this will result in the phase increasing enough to get a good phase margin. Moreover, this can be tuned more precisely to get an exact and optimal result.

Both the Bode diagrams and the step responses of the new tuned system were analysed and compared to the untuned system.

Adding Additional Filters

Even though good control parameters were chosen in the previous section, the system showed unwanted behaviours believed to be a consequence of the large resonance peaks. These resonance peaks were apparent in the Bode plots for both L and LCL grids and resulted in multiple cross-over frequencies. These multiple cross-over frequencies were likely reasons to the problems, such as oscillations, of the system. To counteract this issue, additional filters were added. The following investigations were conducted theoretically, but they were based on the estimated transfer functions. Both the Bode diagrams and the step responses of the systems with additional filters were analysed and compared to the original system.

Lag Compensator. In order to manage the resonance peaks in the Bode plot a lag filter was added to the model, in series with the PI controller. The lag compensator was constructed according to section 2.3.The motivation of adding this filter, was based on the theory that the gain of the frequency response is lowered, resulting in lower maximum values of the resonance peaks.

Notch Filter. Notch filters could be used to manage the resonances. The model of the notch filter was constructed by using the ideas in section 2.3, but with some altering that resulted in a filter of the following form:

$$\frac{s^2 + 2\zeta f_{n1} + f_{n1}^2}{(s + f_{n1})^2} \tag{3.13}$$

The different terms of the filter are ζ, the damping coefficient, and f, the frequency of the maximum value of the resonance peak. The latter was identified through Matlab but the former was separately tuned for each iteration of the grid.

Lead Compensator. It was concluded that the margins of the open loop system with an LCL grid were affected by the notch filter and thus, a lead filter was introduced. The lead filter was designed according to 2.3.

Resonant Compensator. A combination of a resonant compensator and a notch filter was designed in order to remove the resonances completely in the open loop transfer function. These filters were constructed as the following:

$$\frac{f_{n2}^2(s^2 + 2\zeta f_{n1} + f_{n1}^2)}{f_{n1}^2(s^2 + 2\zeta f_{n2} + f_{n2}^2)} \tag{3.14}$$

In this equation f_{n1} refers to the frequency of the maximum value of the upper peak and f_{n2} refers to the frequency of the minimum value of the lower peak. The damping coefficient, ζ, was tuned manually. The peaks were identified through Matlab.

Furthermore, for an LCL grid two of these filters were needed. These were added in series with the open loop system.

3.5 Revising the Control Model to a New Objective

In the mathematical models stated in previous sections, one available measurement signal has been absent, I_{out}. In the present set up of the Simulink model and the real-life product, the control system is working on the objective to minimise the error between I_{adf} and the corresponding set point. However, the real-life end product is in fact I_{out}. This motivates investigations in how the control model could be changed to use all available measurements. The ultimate method in this regard was to reconnect the feedback loop to work on an error between I_{out} and the set point I_{adfsp} instead, resulting in a block diagram showed in Figure 3.8.

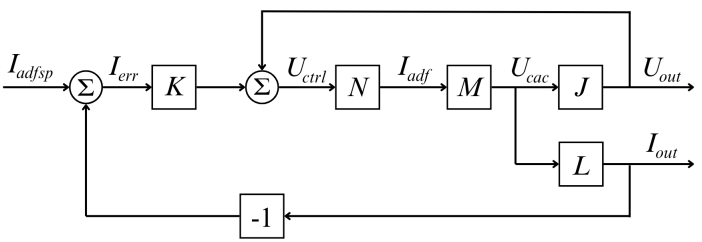

Figure 3.8 Block diagram with feedback loop from I_{out}.

This change was easily implemented into the existing mathematical model and it is shown in Figure 3.9.

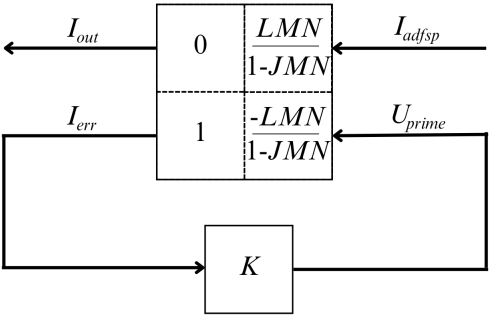

Figure 3.9 Grey box model with feedback loop from I_{out}.

With this setup, the PI controller worked directly on the error between I_{out} and the set point, eliminating steady state error. To further improve the result, the control parameters were tuned and filters added according to section 3.4 with a small adjustment by removing the s from the numerator in the notch filter. However, now I_{adf} was an unused measurement. Different ways to integrate both signals were explored, but it was deemed futile in the scope of this thesis.

4

Result

In this chapter, all the results of this thesis are presented. Since the first sections of Chapter 3 deal with methods of identifying the system and estimating transfer functions, all of these results are presented in section 4.1. In section 4.2 the results needed for validation of the methods are shown. The results regarding PI controller parameter tuning are found in section 4.3, followed by the filter design results in section 4.4, followed by the results of the investigation into new control objectives in section 4.5.

4.1 System Identification

In this section, the results of section 3.1 and 3.2 are showcased. The methods described in these sections all lead up to a complete system estimation that is cross validated between the different versions of obtaining a transfer function.

The result is divided between L and LCL grid. First the estimations of the separate transfer functions of the model are presented together with data points, followed by the combined estimated system together with data points. A data point represents the relationship between the two signals at that specific frequency.

Further on, there will be comparative plots between the combined estimated system and the theoretically calculated system, as well as comparisons between the combined estimated system and the estimated input to output signal system. Comparisons of plots of the transfer function, G, will also be made between the estimations and theoretical calculations.

L Grid

The result of the system identification of L grid is presented below. Standard values of the parameters were used in order to obtain the graphs.

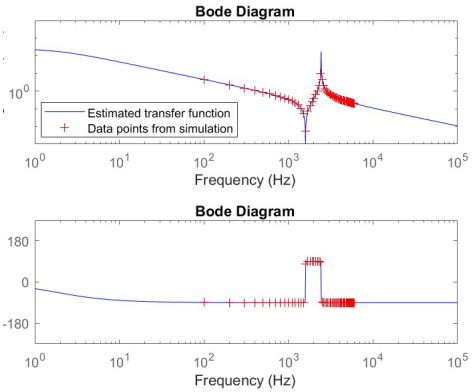

(a) The data points showing the relation between I_{adf} and U_{ctrl} acquired through simulations plotted together with the estimated transfer function between those two signals, N, in a Bode diagram.

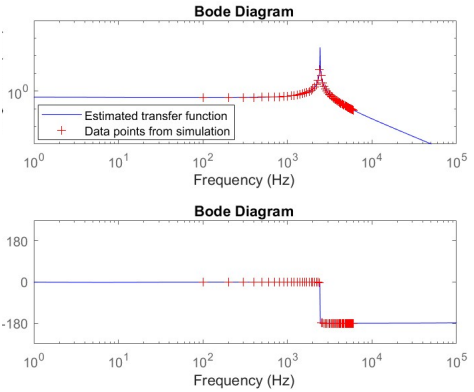

(b) The data points showing the relation between U_{out} and U_{ctrl} acquired through simulations plotted together with the estimated transfer function between those two signals, JMN, in a Bode diagram.

Figure 4.1 The two different transfer functions used in the grey box model (see Figure 3.5).

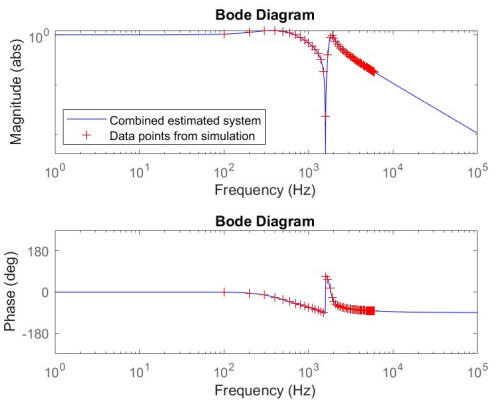

Figure 4.2 Bode diagram of the combined estimated system and the data points showing the relation between the input signal and output signal of the simulated complete system.

By using the methods described in section 3.2, both a transfer function directly from input signal to output signal and a transfer function of the combined estimated system were acquired and they are compared below.

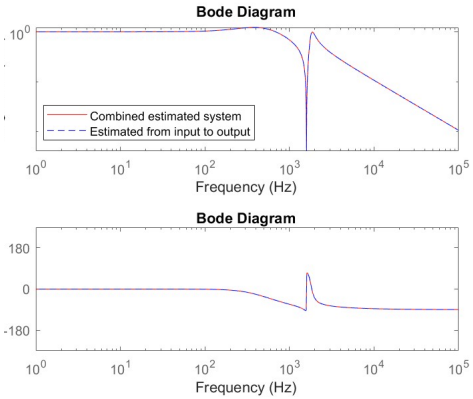

(a) Bode diagram of the combined estimated system and the estimated transfer function from input to output signal.

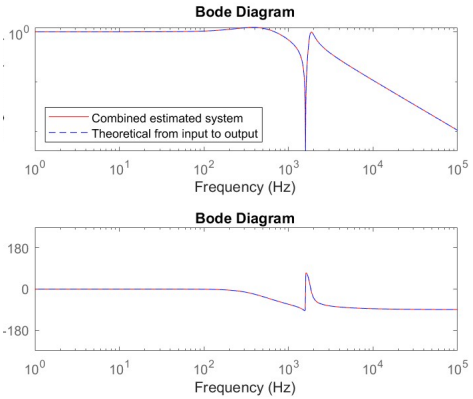

(b) Bode diagram of the combined estimated system and the theoretically calculated transfer function from input to output signal.

Figure 4.3 Comparisons between estimations and theoretically calculated transfer functions.

The same comparison was made for the process G.

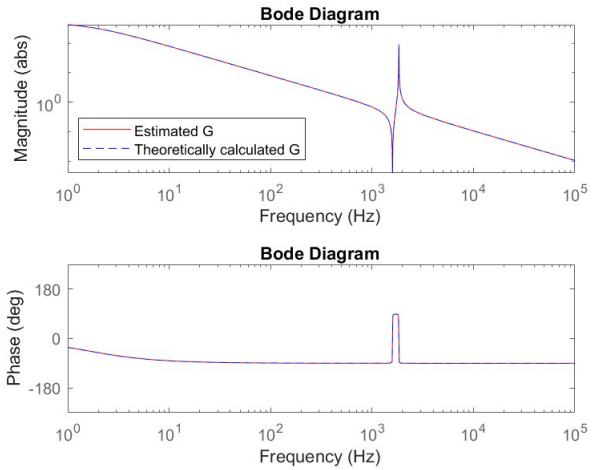

Figure 4.4 Bode diagram of estimated transfer function, G, and theoretically calculated transfer function, G.

The estimated transfer function, G, is the following:

$$G = \frac{1060.9(s^2 + 3.182s + 2.532e06)}{(s + 1.592)(s^2 + 2.917s + 3.376e06)} \tag{4.1}$$

LCL Grid

The result of the system identification of LCL grid is presented below. Standard values of the grid parameters, except Lg1=300 H, were used in order to obtain the graphs.

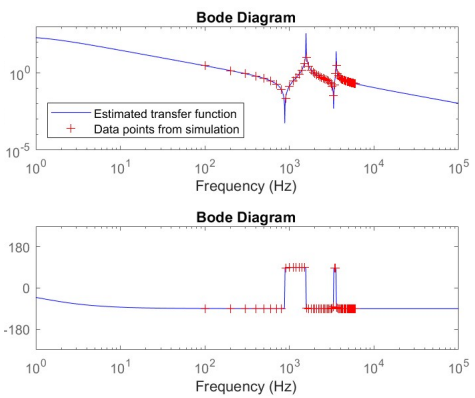

(a) The data points showing the relation between I_{adf} and U_{ctrl} acquired through simulations plotted together with the estimated transfer function between those two signals, N, in a Bode diagram.

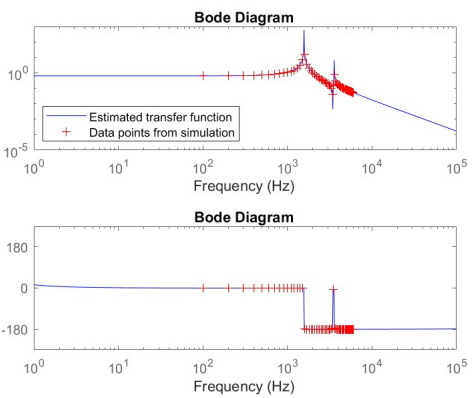

(b) The data points showing the relation between U_{out} and U_{ctrl} acquired through simulations plotted together with the estimated transfer function between those two signals, JMN, in a Bode diagram.

Figure 4.5 The two different transfer functions used in the grey box model (see Figure 3.5).

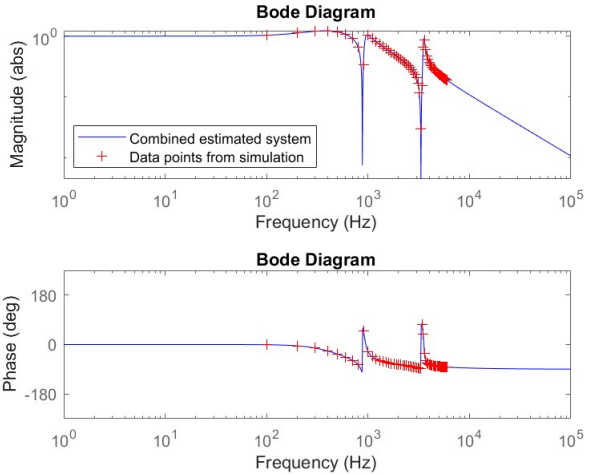

Figure 4.6 Bode diagram of the combined estimated system and the data points showing the relation between the input signal and output signal of the simulated complete system.

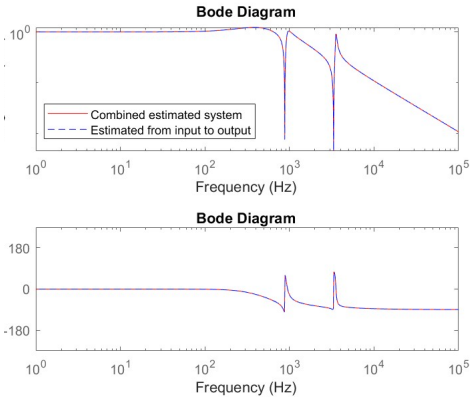

(a) Bode diagram of the combined estimated system and the data points showing the relation between the input signal and output signal of the simulated complete system.

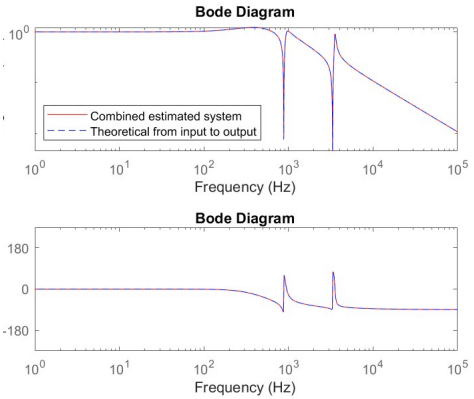

(b) Bode diagram of the combined estimated system and the theoretically calculated transfer function from input to output signal.

Figure 4.7 Comparisons between estimations and theoretically calculated transfer functions.

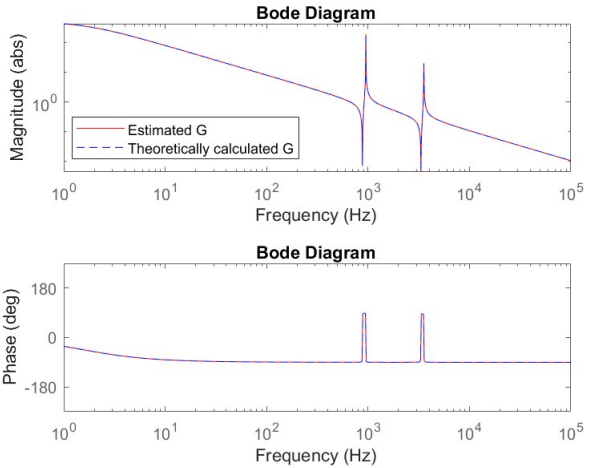

Figure 4.8 Bode diagram of estimated transfer function, G, and theoretically calculated transfer function, G.

The estimated transfer function, G, is the following:

$$G = \frac{1061(s^2 + 1.005s + 7.744e05)(s^2 + 6.416s + 1.105e07)}{(s + 1.592)(s^2 + 0.7205s + 9.049e05)(s^2 + 6.699s + 1.26e07)} \tag{4.2}$$

4.2 Validating Results

The results used for validation as described in section 3.3 are presented below. First of all, comparisons between pole-zero maps of the theoretically calculated and the estimated transfer functions, both with and without Matlab's tool of pole-zero cancellation (*minreal()*), are presented. This is followed by thorough comparisons between theoretically calculated and estimated transfer functions when varying grid parameters. After that, a table containing calculated NRMSE values for different grid iterations is shown. Finally, a table containing comparisons using the gap metric is presented.

Pole-Zero Map and Need for Pole-Zero Cancellation

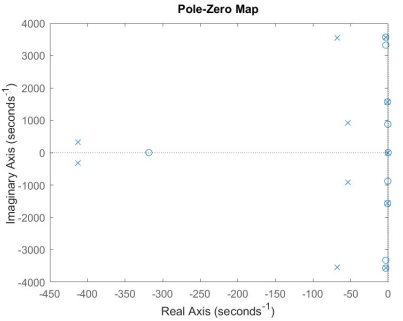

(a) Pole-zero map of estimated transfer function (CES) without using *minreal()*.

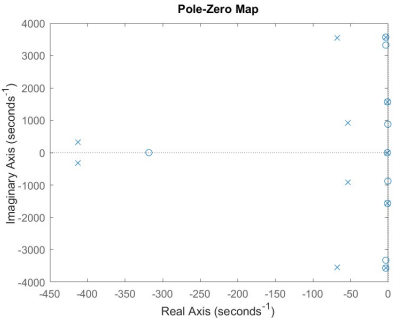

(b) Pole-zero map of theoretically calculated transfer function without *minreal()*.

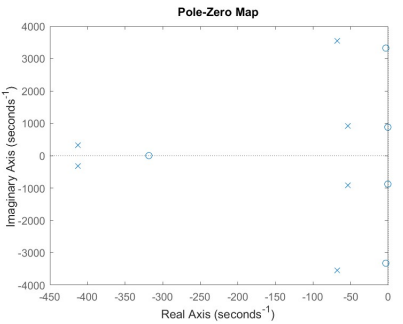

(c) Pole-zero map of estimated transfer function (CES) with tolerance of 0.0001 in *minreal()*.

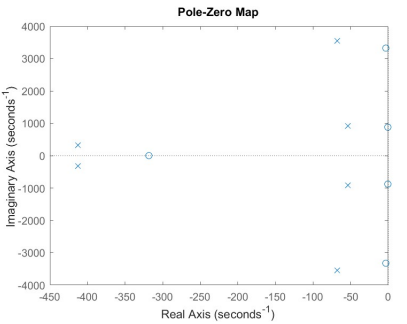

(d) Pole-zero map of theoretically calculated transfer function with tolerance of 0.0001 in *minreal()*.

Figure 4.9 Pole-zero map of complete system from I_{adfsp} *to* I_{adf}.

***Estimations with Different Tolerances in* minreal().** The following three estimated transfer functions have the standard grid parameters except for Cg1=300 F and Lg1=300 H in an LCL grid.

Theoretically Calculated Transfer Function

$$\frac{1061(s+318.3)(s^2+0.9431s+2.395e05)(s^2+6.484s+5.952e06)}{(s^2+822.1s+2.679e05)(s^2+12.75s+2.393e05)(s^2+235.2s+7.512e06)} \tag{4.3}$$

Estimated Transfer Function with Tolerance 0.1

$$\frac{1061(s+318.3)(s^2+0.9459s+2.395e05)(s^2+6.483s+5.952e06)}{(s^2+821.9s+2.68e05)(s^2+12.75s+2.392e05)(s^2+235.2s+7.512e06)} \quad (4.4)$$

Estimated Transfer Function with Tolerance 0.0001

$$\frac{1061(s+318.3)(s^2+0.9459s+2.395e05)(s^2+2.218s+5.817e05)(s^2+6.483s+5.952e06)}{(s^2+821.9s+2.68e05)(s^2+12.75s+2.392e05)(s^2+2.22s+5.817e05)(s^2+235.2s+7.512e06)} \quad (4.5)$$

Varying Values of Components for Validation

The following equations show the transfer functions of the complete system with other values of components than the standard grid parameters. Each subsection shows which component deviates from its standard value and in what type of grid. The first equation is the theoretically calculated transfer function and the second is the estimated one, enabling direct and exact comparison.

Lg1=50 H in L grid.

Theoretically Calculated Transfer Function.

$$\frac{1061(s^2+4.244s+3.377e06)}{(s+1.592)(s^2+4.067s+4.503e06)} \quad (4.6)$$

Estimated Transfer Function

$$\frac{1061(s^2+4.244s+3.377e06)}{(s+1.592)(s^2+4.067s+4.502e06)} \quad (4.7)$$

Lg1=200 H in L grid.

Theoretically Calculated Transfer Function

$$\frac{1061(s^2+2.122s+1.689e06)}{(s+1.592)(s^2+1.768s+2.252e06)} \quad (4.8)$$

Estimated Transfer Function

$$\frac{1060.9(s^2+2.121s+1.688e06)}{(s+1.592)(s^2+1.767s+2.25e06)} \quad (4.9)$$

Lg1=50 H in LCL grid.

Theoretically Calculated Transfer Function

$$\frac{1061(s^2+4.115s+2.968e06)(s^2+8.617s+1.73e07)}{(s+1.592)(s^2+3.945s+3.762e06)(s^2+8.788s+1.819e07)} \tag{4.10}$$

Estimated Transfer Function

$$\frac{1061(s^2+4.115s+2.968e06)(s^2+8.615s+1.729e07)}{(s+1.592)(s^2+3.944s+3.762e06)(s^2+8.786s+1.819e07)} \tag{4.11}$$

Lg1=100 H in LCL grid.

Theoretically Calculated Transfer Function

$$\frac{1061(s^2+2.639s+1.935e06)(s^2+6.91s+1.326e07)}{(s+1.592)(s^2+2.347s+2.355e06)(s^2+7.202s+1.453e07)} \tag{4.12}$$

Estimated Transfer Function

$$\frac{1061(s^2+2.639s+1.935e06)(s^2+6.908s+1.326e07)}{(s+1.592)(s^2+2.347s+2.355e06)(s^2+7.201s+1.453e07)} \tag{4.13}$$

Cg1=150 F in LCL grid.

Theoretically Calculated Transfer Function

$$\frac{1061(s^2+2.568s+1.177e06)(s^2+6.982s+7.266e06)}{(s+1.592)(s^2+2.521s+1.29e06)(s^2+7.029s+8.842e06)} \tag{4.14}$$

Estimated Transfer Function

$$\frac{1061(s^2+2.567s+1.177e06)(s^2+6.981s+7.266e06)}{(s+1.592)(s^2+2.521s+1.29e06)(s^2+7.028s+8.842e06)} \tag{4.15}$$

Cg1=300 F in LCL grid.

Theoretically Calculated Transfer Function

$$\frac{1061(s^2+2.761s+7.073e05)(s^2+6.788s+6.047e06)}{(s+1.592)(s^2+2.78s+7.404e05)(s^2+6.769s+7.703e06)} \tag{4.16}$$

Estimated Transfer Function

$$\frac{1061(s^2+2.761s+7.073e05)(s^2+6.787s+6.047e06)}{(s+1.592)(s^2+2.78s+7.404e05)(s^2+6.768s+7.703e06)} \tag{4.17}$$

NRMSE

The table below shows the results of the NRMSE calculations when comparing the estimated transfer function from input to output with the data points and when comparing the combined estimated system with the data points.

Table 4.1 NRMSE values of estimations on different grids, for both the estimated input to output transfer function and the combined estimated system.

Type of grid	Parameter changed	NRMSE for I/O	NRMSE for CES
L	Lg1=50e-6 H	99.9978%	99.8991%
L	Lg1=100e-6 H	99.9977%	99.8924%
L	Lg1=200e-6 H	99.9977%	99.8788%
LCL	Lg1=50e-6 H	99.9978%	99.9020%
LCL	Lg1=100e-6 H	99.9978%	99.9035%
LCL	Lg1=300e-6 H	99.9977%	99.9015%
LCL	Cg1=50e-6 F	99.9978%	99.9035%
LCL	Cg1=150e-6 F	99.9978%	99.9024%
LCL	Cg1=300e-6 F	99.9978%	99.9020%

Gap Metric

The table below contains the gap metric of estimations of G on different grids calculated through the method described in section 3.3. The table shows which type of grid was simulated and what change it had been subjected to compared to the standard grid parameters.

Table 4.2 The gap metric between the estimated process, G, and the theoretically calculated process, G.

Type of grid	Parameter changed	Gap metric
L	Lg1=50e-6 H	0.0017
L	Lg1=100e-6 H	0.0030
L	Lg1=200e-6 H	0.0044
LCL	Lg1=50e-6 H	0.0097
LCL	Lg1=100e-6 H	0.0041
LCL	Lg1=300e-6 H	0.0024
LCL	Cg1=50e-6 F	0.0041
LCL	Cg1=150e-6 F	0.0010
LCL	Cg1=300e-6 F	0.00070

Gap Metric of Estimations on Signals with Added Noise

The table below shows the gap metric of the process, G, when the voltage U_{ctrl} was subjected to white noise, compared to the theoretically calculated G without noise.

Table 4.3 The gap metric between the estimated process, G, from simulations where the signals were subjected to noise, and the theoretically calculated process, G.

Noise power	Maximum value of noise	Gap metric
0.01	448.9008	0.9984
0.001	148.8935	1
0.0001	54.0228	0.0723
0.00001	24.0221	0.0231

Nyquist Plots of G

The following figures show the Nyquist plots of the theoretically calculated process, G, and the open loop system with controller, $G \cdot K$. The standard values for an LCL grid were used to obtain these plots.

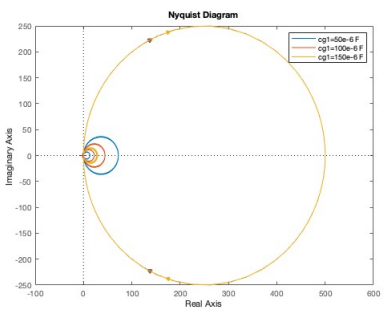

Figure 4.10 Nyquist diagram of process, G, with varying value of Cg1.

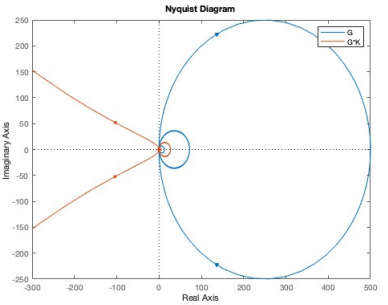

(a) Nyquist diagram of G and $G \cdot K$.

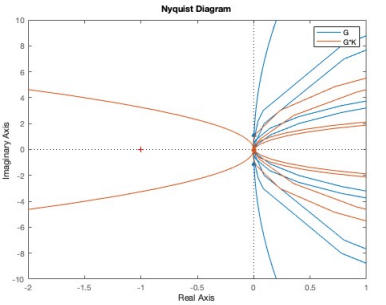

(b) Close-up of Nyquist diagram of G and $G \cdot K$.

Figure 4.11 The Nyquist diagrams of G and $G \cdot K$ with standard parameter values.

4.3 PI Controller Design

The following figures show the result of tuning the PI controller parameters according to section 3.4. The requirement on bandwidth was set to 300 Hz for an LCL grid. Standard grid parameters were used, with the exception of Lg1=300 H. The Bode diagrams show the system after each step in the tuning procedure with the final plot showing the closed loop system.

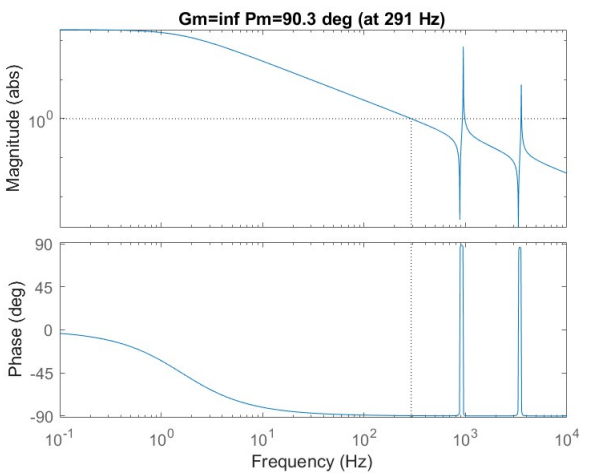

Figure 4.12 Bode diagram of $G \cdot K$ where $Kp = \frac{1}{|G(300j)|}$ and $Ki = 0$.

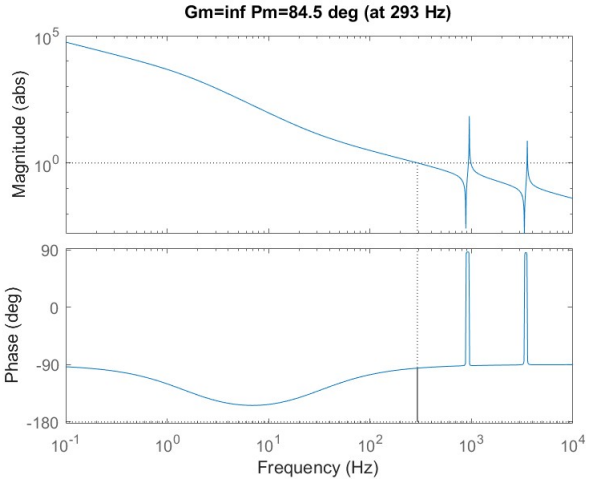

Figure 4.13 Bode diagram of $G \cdot K$ where $Kp = \frac{1}{|G(300j)|}$ and $Ki = 30Kp$.

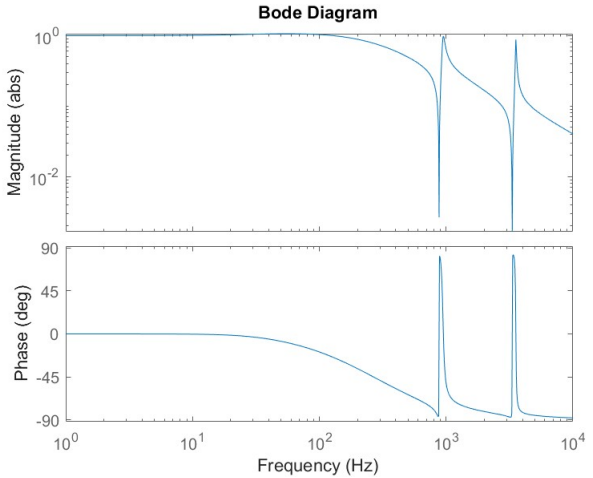

Figure 4.14 The closed loop transfer function, $\frac{GK}{1+GK}$, with $Kp = \frac{1}{|G(300j)|}$ and $Ki = 30Kp$ and bandwidth $f_b \approx 318$ Hz.

Sensitivity Function. The following figure shows the sensitivity function of the system with a tuned PI controller:

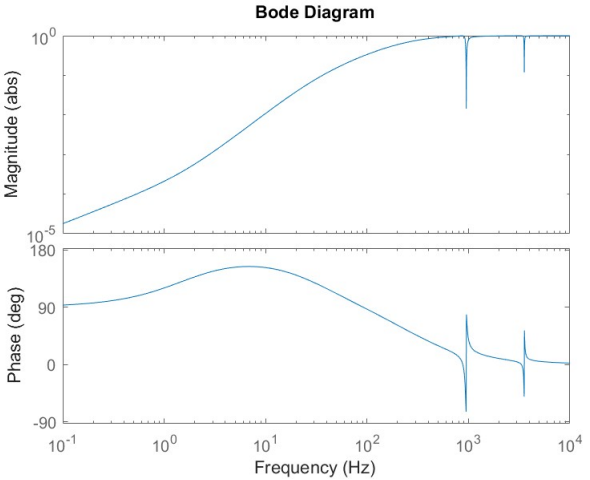

Figure 4.15 The sensitivity function, $\frac{1}{1+GK}$, with $Kp = \frac{1}{|G(300j)|}$ and $Ki = 30Kp$.

4.4 Filter Design

The results obtained from the filter design method in section 3.4 are presented below. First of all, the Bode diagram of the filter is shown, followed by the Bode diagrams of the open loop complete system with added filter. After that, the Bode diagram of the closed loop complete system with added filter is presented. These results will first be shown for an L grid and then an LCL grid. For the LCL grid, results will be shown both with a configuration of a notch and lead filter, and then a configuration of a notch filter and resonant compensator. Finally, a step response of the closed loop system of an LCL grid with all configurations is shown.

L Grid

The standard values of the grid parameters and the transfer function of the estimated process, G, were used. Furthermore, the PI controller was tuned according to section 3.4.

Notch Filter. The following figures show the Bode diagrams when incorporating a notch filter in the system:

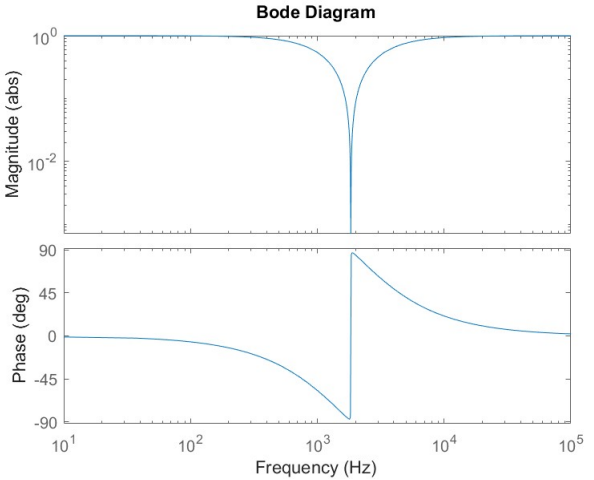

Figure 4.16 Bode diagram of notch filter, $N1$.

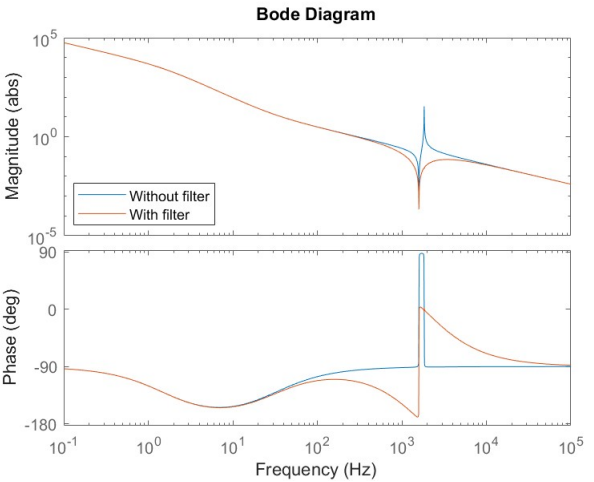

Figure 4.17 Bode diagram of the open loop system with added notch filter, $G \cdot K \cdot N1 \Rightarrow f_c \approx 284$ Hz, compared to the Bode diagram of the system without the filter.

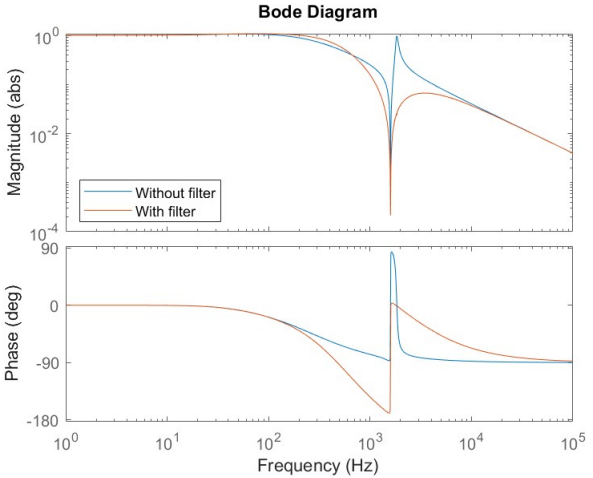

Figure 4.18 Bode diagram of the closed loop system with added notch filter, $\frac{G \cdot K \cdot N1}{1+G \cdot K \cdot N1} \Rightarrow f_b \approx 426$ Hz, compared to the Bode diagram without filter.

LCL Grid

The standard values of the grid parameters, except Lg1=300 H, and the transfer function of the estimated process, G, were used. Furthermore, the PI controller was tuned according to section 3.4.

Notch Filters With a Lead Filter. The following figures show the Bode diagrams when incorporating notch filers and a lead filter in the system.

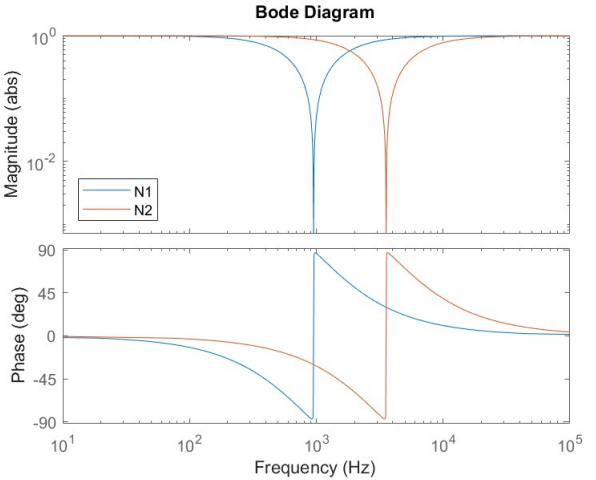

Figure 4.19 Bode diagram of notch filters, $N1$ and $N2$.

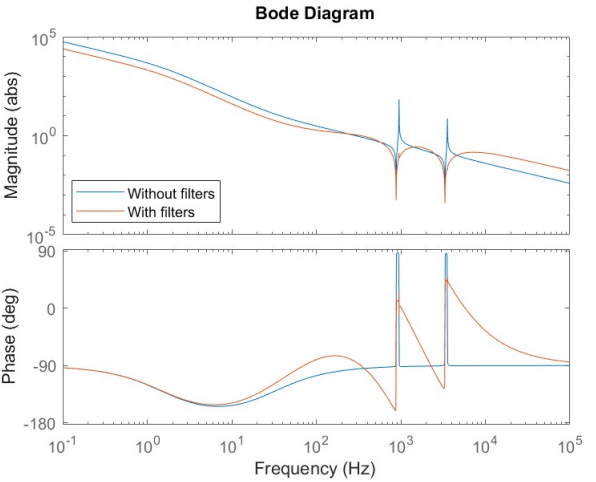

Figure 4.20 Bode diagram of the open loop system with added notch filters and a lead compensator (L), $G \cdot K \cdot N1 \cdot N2 \cdot L \Rightarrow f_c \approx 337$ Hz, compared to the Bode diagram of the system without the filters.

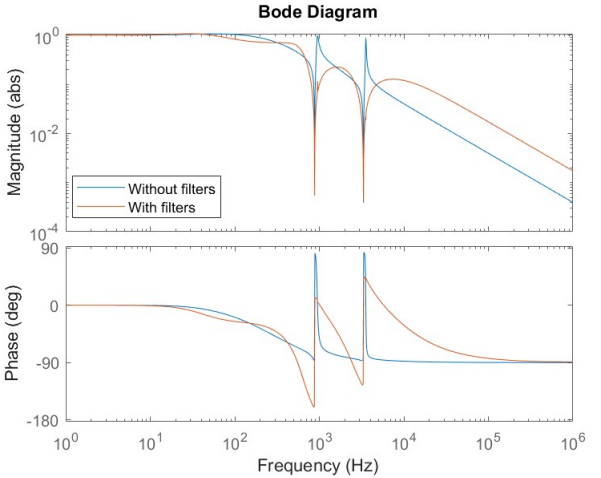

Figure 4.21 Bode diagram of the closed loop system with added notch filters and a lead compensator, $\frac{G \cdot K \cdot N1 \cdot N2 \cdot L}{1+G \cdot K \cdot N1 \cdot N2 \cdot L} \Rightarrow f_b \approx 286$, compared to the Bode diagram without added filters.

Notch Filter with Resonant Compensator. The following figures show the Bode diagrams when incorporating a notch filter and a resonant compensator in the system.

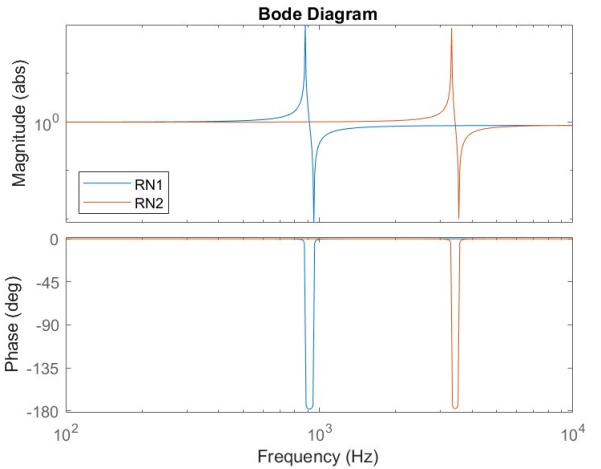

Figure 4.22 Bode diagram of filters, *RN*1 and *RN*2.

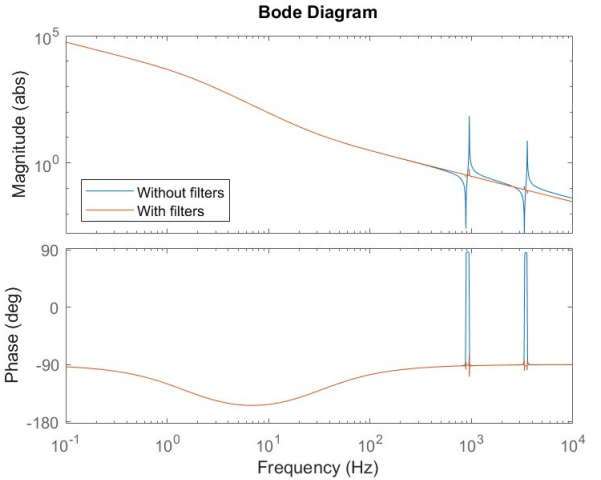

Figure 4.23 Bode diagram of the open loop system with added filters, $G \cdot K \cdot RN1 \cdot RN2 \Rightarrow$ 298 Hz, compared to the system without added filters.

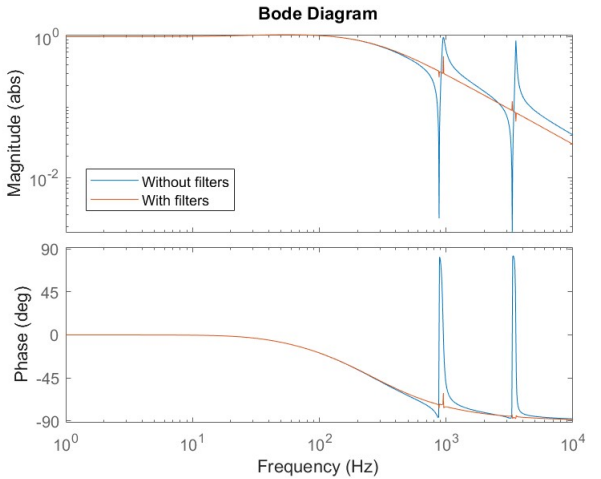

Figure 4.24 Bode diagram of the closed loop system with added filters, $\frac{G \cdot K \cdot RN1 \cdot RN2}{1+G \cdot K \cdot RN1 \cdot RN2} \Rightarrow$ $f_b \approx 324$, compared to the system without added filters.

Step Response

The standard values of the grid parameters, except Lg1=300 H, and the transfer function of the combined estimated system were used to obtain the following step

response:

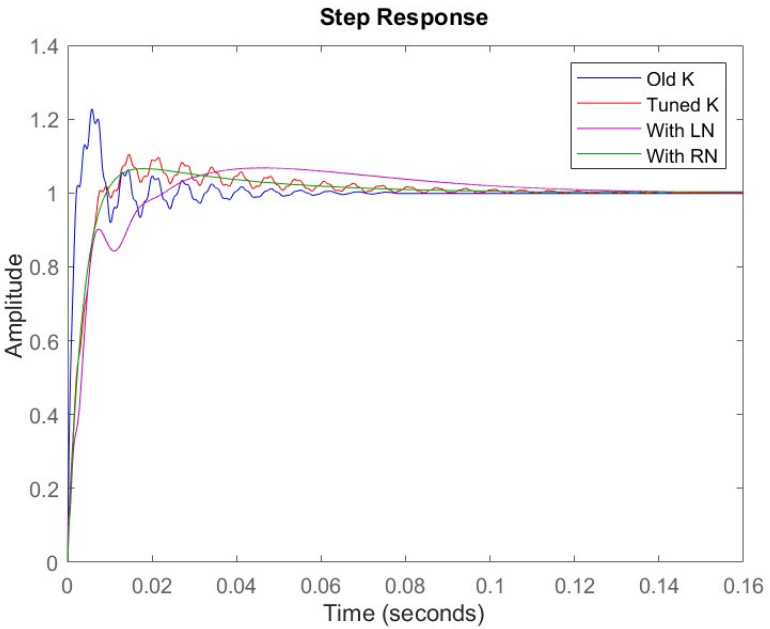

Figure 4.25 Step response of the closed loop system with the standard PI controller (Old K), with the tuned PI controller (Tuned K) and with the tuned PI controller in combination with the specified filter (lead compensator and notch filters, LN, or resonant compensators and notch filters, RN).

4.5 Revised Control Model

The results obtained from section 3.5 are presented below. First a Bode diagram of the transfer function between the signals I_{adf} and I_{out}, then the filter design used on the new closed loop system with feedback from I_{out} instead of I_{adf}. This is followed by Bode diagrams showing both open loop and closed loop systems with and without filter added. Finally, the step responses of the closed loop system is also presented with and without added filter.

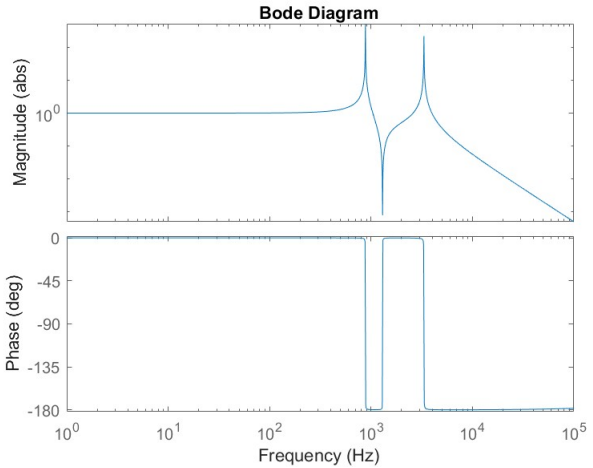

Figure 4.26 Bode diagram of the estimated transfer function from I_{adf} to I_{out}.

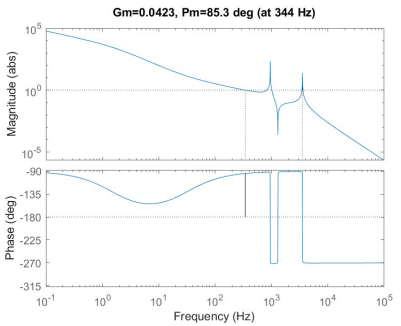

(a) Bode diagram of the open loop system transfer function from I_{adfsp} to I_{out}.

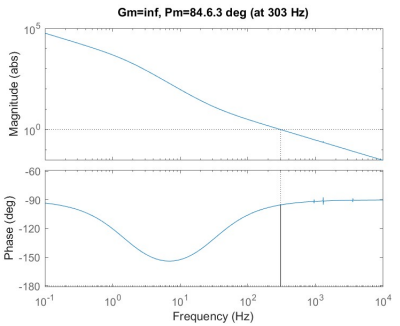

(b) Bode diagram of the open loop system transfer function from I_{adfsp} to I_{out} with added notch filters and resonant compensator.

Figure 4.27 The open loop system, with and without added notch filters and resonant compensator.

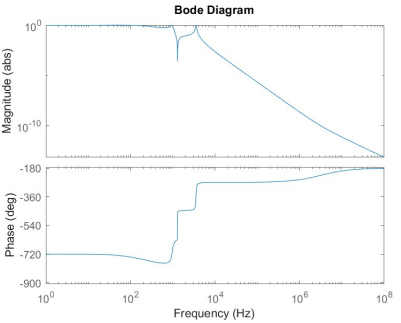

(a) Bode diagram of the closed loop system transfer function from I_{adfsp} to I_{out}.

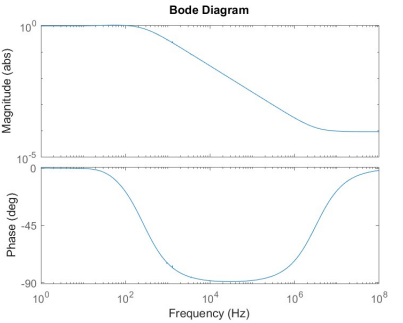

(b) Bode diagram of the closed loop system transfer function from I_{adfsp} to I_{out} with added notch filters and resonant compensator.

Figure 4.28 The closed loop system, with and without added notch filter and resonant compensator.

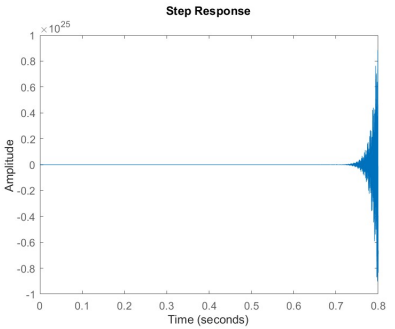

(a) Step response of the closed loop system from I_{adfsp} to I_{out}.

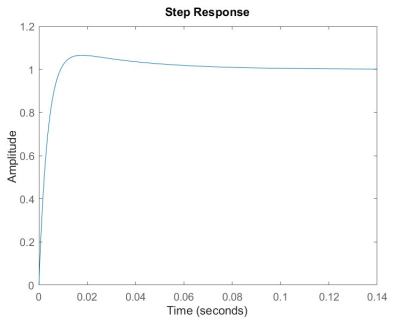

(b) Step response of the closed loop system from I_{adfsp} to I_{out} with added notch filters and resonant compensator.

Figure 4.29 Step response of closed loop system from I_{adfsp} to I_{out}, with and without notch filter and resonant compensator.

5

Discussion

The desired result of this thesis is the specific workflow regarding identifying the behaviour and analysing the stability and robustness of the active dynamic filtering system, and as a result finding parameters of the controller to obtain desired system behaviour. This section is a discussion about this workflow, the specific results of Chapter 4 and the problem formulations.

With the set limitations in the problem formulations and with the simulated environment on which the experiments were conducted, the questions stated in the problem formulation in section 1.2 have been answered in a satisfactory way. The method that was chiselled out throughout the experiments and presented in Chapter 3, is a method which can identify a system consisting of a controller, a filter and a grid, depending on solely accessible data, solving the first problem.

An investigation, as of problem 2 in section 1.2, has also been conducted focusing on how to tune the control parameters to achieve a certain bandwidth and phase margin. The analysis was also extended into the advantages of adding potential filters. However, the results are largely dependent on the imposed limitations and the effects will be discussed in length below.

5.1 Validity of Result

The method to estimate the different transfer functions was tested on two different types of grids, a solely inductive grid (L grid) and an inductive-capacitive grid (LCL grid). These were specified by Comsys as the two most important categories of grids that would make the resulting workflow as useful as possible in real life implementation.

The workflow and methods were first constructed on data from an L grid and was then quite smoothly transferred into data from an LCL grid. The adjustment required

for the estimation method to accommodate for an LCL grid was to replace the requested degrees of the transfer functions in Matlab's *pem()* function. Since LCL grids have new characteristics, a natural consequence is that the resulting transfer functions have different degrees than for an L grid. The fact that the method was able to obtain successful approximations of transfer functions in both these cases increases the reliability of this method. Since all L and LCL grids retain the same order and character of their system transfer functions, the workflow is expected to cover all possible iterations of grid parameters in these categories.

However, if a new type of grid would be required to be examined, either the theoretical steps presented in section 3.2: *Identifying Relationships of Signals* could be performed, or the more general *tfest()* function in Matlab's system identification toolbox could be used as presented in 3.2: *Estimation of Transfer Function*. Through these methods, a new expected degree could be produced and used in the estimation method primarily employed and presented in this thesis. The function *tfest()* namely does not need the prior knowledge that *pem()* requires with the consequence that transfer functions of completely wrong order might be fitted to the data.

Changing Parameter Values. To further validate the result and the versatility of the workflow, the method was tested on different values of the grid. The values of Lg1 or Cg1 were changed while the rest were kept as the standard grid parameters (seen Appendix 8.1). These iterations of parameters are seen as reasonable changes since it is the impedances of the grid that would vary in reality. The parameters of the low pass filter can be assumed to be known, with some certainty, in real life and thus, those were not tested for different values. The result of section 4.2 shows how transfer functions, similar to the ones theoretically expected, are successfully estimated each time. This further indicates that this method is valid. As can be seen in Table 4.1, the normalised root mean square error of the estimated transfer functions compared to the data points of the simulations stays above 99% for all the different tested configurations.

To understand how well the estimated process corresponded to the theoretically calculated process G, gap metric was also used as seen in Table 4.2. As gap metric is a measure of distance between models. The results show that the estimated transfer function is very close to the theoretical one, throughout all iterations of parameters. This shows that the estimated system is accurate in the sense that it is possible to design a controller for the estimated transfer function in order to get the wanted result on the actual system. However, this was the results from an idealised environment.

Furthermore, it is important to acknowledge that it is the comparisons of the process G which are the most important when iterating parameters. The behaviour of the estimated process might be hidden if a controller was incorporated in the estimations.

Therefore, it is also interesting to observe the Nyquist diagram of the process and the open loop process connected to controller in Figure 4.10 and Figure 4.11. The magnitude of the process increases when increasing the values of the grid inductance, but the entire plot stays in the RHP and the process is passive and stable. Not until the controller is attached, the Nyquist diagram exists in the LHP and the risk of unstable margins appears.

Pole-Zero Cancellation and Estimation Error. For an even further examination of the validity of the estimations, poles and zeros of the estimated system compared to those of the theoretically calculated system (see Figure 4.9) were observed. These results also show the importance of using Matlab's *minreal()* function for pole-zero cancellation. For the theoretical transfer functions, it is necessary to shorten the fractions since Matlab does not cancel factors with the same values in order to avoid rounding errors. For the estimations it is further useful in order to cancel estimation errors, in addition to similar numerical issues.

A tolerance of 0.1 in *minreal()* was sufficient in order to cancel pole and zero pairs of the estimated transfer functions to match the theoretical ones. The importance of a higher tolerance is shown in equations 4.4 and 4.5. A tolerance of 0.1 is still quite low and it is a reasonable tolerance to use. By observing the transfer functions in section 4.2, it was concluded that all unique poles and zeros are located at a large distance from each other. Thus, *minreal()* will not create a problem by cancelling too many poles even with larger tolerance. In Figure 4.9 the importance of *minreal()* is shown in both the case of correctly shortening the fractions, and in the case of counteracting estimation errors.

Effects of Noise in Signal in Simulations. To further test the method of estimations, noise was added to the control signal in the simulations and from that data the method was used to estimate the process G. Table 4.3 shows the gap metric between those estimations, and the theoretically calculated transfer function. Additionally, there is a column containing the maximum value of the noise signal. These are the maximum value added to the voltage U_{ctrl} by the noise generator and can be compared to U_{ctrl} itself, which varies by 2 V around 10 V.

Since noise powers 0.01 and 0.001 indicate that numbers way larger than the signal were added to U_{ctrl}, it seems reasonable that the gap metrics of the following estimations were large. However, the other noise powers resulted in reasonably small gap metrics and thus, it can be concluded that the model is robust to noise of that power level. In order to make the model even more robust to noise, some kind of filter could be added to the data before it is used in the estimations. However, since the resonance peaks also cause outliers in the data it is not obvious how such a filter would be constructed. Additional information about the noise level is needed to analyse necessary changes to the estimation methods to handle the noise present in the system in reality.

5.2 Tuning PI Parameters

With valid results of estimations of the process, focus could shift to investigating how to tune the parameters of the PI controller. As discussed above, the process G is stable. Thus, the main interest of adding a PI controller to the system is not to stabilise the system, but rather to obtain a certain bandwidth with robust stability margins.

Tuning the PI parameters based on the method described in 3.4 was shown to be a good strategy. This is due to the fact that the system behaved like a fairly simple system for frequencies lower than the resonance peaks, which was supported by the transfer functions shown in section 4.3. This indicates that if the desired bandwidth is located at a lower frequency than the resonance peaks the assumption that the phase margin is -90° at the cross-over frequency is reasonable. Thus, the tuning method, based on raising the gain by choosing K_p as $\frac{1}{|G(jf_b)|}$ and then choosing K_i as $0.1 \cdot f_b \cdot K_p$ for a good location of the corner frequency, could be employed. The motivation to these choices are explained in the theory of section 2.3, but the results show that these choices clearly provide the required bandwidth with good margins for this system.

With the original parameters of the PI controller the bandwidth for an LCL grid with Lg1=300 H was closer to the resonance peaks, causing oscillations in the step response. With a bandwidth of 300 Hz, which is safely located before the peaks, oscillations of the step response were notably smaller, as can be seen in Figure 4.25.

The sensitivity function and the complementary sensitivity function of the system are shown in Figure 4.15 and Figure 4.14 respectively. The gain of the sensitivity function is small for low frequencies, which shows that the system has disturbance rejection for those frequencies. The maximum sensitivity never exceeds 2, which follows the rule of thumb described in section 2.3 that guarantees robust stability margins. Furthermore, the gain of the complementary sensitivity function is low for high frequencies, in accordance with theory in section 2.3. For further examination more information regarding what kind of disturbances and measurement noise the system is subjected to in reality is necessary.

5.3 Necessity of Additional Filters

As seen in the Bode diagrams of section 4.1, the capacitive features of the electrical system give rise to resonance peaks, one resonance in the case of a completely inductive grid (L grid) and two resonances if there exists a capacitor in the grid as well (LCL grid). These peaks causes oscillations to appear in the step response (see

Figure 4.25). This is naturally not a desirable behaviour of the system and therefore, it would be preferable to have some kind of feature that nullifies these peaks.

The peaks result in multiple cross-over frequencies that create the issue of oscillations, which is problematic. The contribution from the peaks will not cause such problems if the maximum value has a gain lower than one. This objective is reached with a simple PI controller if the bandwidth is very small. However, this trade-off with the real control objective of a large bandwidth is unacceptable and therefore, investigations continued into other ways of removing the influence of the peaks.

An alternative way of removing the impact of the peaks is with the help of filters. This was tested according to the method described in section 3.4. First of all, a lag compensator was designed according to the rules of thumb, described in section 2.3 with the goal of lowering the gain of all frequencies larger than the cross-over frequency. However, it was discovered that a lag compensator was not sufficient to remove the multiple cross-over frequencies caused by the peaks.

Secondly, a notch filter was designed to handle the peaks. This gave good results for an L grid, but the margins were negatively affected for an LCL grid. However, adding a lead filter could solve that problem. Because of the narrow peaks in the notch filter, it was important to obtain a fairly precise measurement of the frequency of the maximum values of the peaks in order to get the best attenuation. When these frequencies were confirmed, there was a need for a lot of damping, ζ, in order to attenuate the resonances, otherwise the filters themselves overcompensated for the peaks in the full system. A damping around $\zeta = \frac{1}{1000}$ was found to be sufficient. However, it was the ideal environment that made it possible to minimise the resonances to that extent. The filter was tailor made to the peaks and a miscalculation of the peaks would cause new problems to arise.

After that, a filter consisting of a resonant compensator in combination with a notch filter was designed according to section 2.3. It consisted of one part cancelling out the lower peak, and one part cancelling out the higher peak of the total resonance behaviour. The result shown in section 4.23 are Bode diagrams of the frequency response of both type of grids together with calculated control parameters and an added combination of notch filter and resonant compensator. As seen in these plots, the filter almost completely rejects the peaks. This in turn results in a unique cross-over frequency and furthermore, in a step response with a more smooth rise to the reference value (see Figure 4.25). However, the resonant compensator is in itself a resonance and adding more resonances to the system is not preferable since small miscalculations would be detrimental to the entire system.

5.4 Revising the Control Model

The ADF system produced by Comsys has the target of creating a stable current as the output after a high frequency filter. Even though the present control system works on the current I_{adf} (the current before the high frequency filter), it is actually I_{out} (the current after the high frequency filter) that is of a greater interest. Thus, I_{out} should follow the reference value of the control system (see figure in Appendix 8.2). In the future, this current will be measurable as well. Therefore, it is of interest to investigate a method that controls I_{out} directly, instead of controlling I_{out} indirectly by solely controlling I_{adf}. This subject was touched upon in this thesis with the results presented in section 4.5.

The major change between this new system, where the objective was to control I_{out}, and the previous system is the feedback signal which was changed to I_{out} from I_{adf}. Thus, an estimation of this transfer function was necessary. The Bode diagram of that transfer function (see Figure 4.27a) also shows that $I_{adf} \approx I_{out}$ before the resonance peaks, making it plausible that the system should be able to be controlled in a similar way, as well as confirming why it has previously been possible to control the system with just the measurement of I_{adf}.

The Bode diagram from I_{adfsp} to I_{out} can be seen in Figure 4.27a. This is the frequency response of the open loop system that consists of the controller, and the estimated transfer function from U_{prime} to I_{out}. The desired cross-over frequency was achieved by tuning the control parameters according to the same procedure as before. However, the gain margin is very low which indicates that the system is unstable.

Furthermore, when the loop was closed, the system behaviour changed drastically. Figure 4.28a shows how the phase of the system starts out at -720° and rises by 540° degrees to -180°. When observing the step response of this system (see Figure 4.29a), it is concluded that this system is unstable. After investigating possible reasons, it was deduced that the resonance peaks played an even more detrimental part and abrupted the stability of the system. This could be counteracted with resonant compensators in combination with notch filters, eliminating the resonance peaks and stabilising the system. The comparisons between Bode diagrams with and without filters are made in Figures 4.28a and 4.28b and between step responses in Figures 4.29a and 4.29b.

The results of these investigations indicate that in order to control the system working on an error between a reference value and the current leaving the ADF system (I_{out}), it is crucial that the impact of the resonance peaks is handled. However, this way of adding a resonance to the system is precarious and other ways of removing the impact of the capacitive behaviour in the Bode diagrams should be examined.

5.5 Limitations in Model of the Grid

As mentioned, this thesis was limited to two types of grids, namely an L grid and an LCL grid. This was a fairly accurate approximation. Nevertheless, the major necessary changes of the method to accommodate for a new type of grid were described in section 5.1. Moreover, a major part of the system identification when using the function *pem()*, is that it is known beforehand whether the grid can be approximated to an L or an LCL grid. However, one way of not having to rely on this is to first plot the data and identify the resonance peaks. As can be seen in the Bode diagrams in sections 4.1 there is one resonance for an L grid and there are two resonances for an LCL grid. In real life it is probable that similar differences between them is present in the Bode diagrams, which would make it easy to differentiate which approximation that should be used in the situation.

Further significant restrictions in this thesis were the absence of disturbances and measurement noise. These factors will have a significant impact on the estimations in reality. Nevertheless, this was outside the scope of this thesis.

5.6 Real-Life Implementation

The goal described by Comsys, and the motivation for this thesis, is that the presented workflow eventually will be implemented in real life. This section is a discussion about how this can be done and problems that may occur.

The Matlab function *pem()* was employed to fit functions in the estimation method. In order to implement this function in another programming language, with the ability to run on small computing power, implementation from scratch is necessary. This is regarded as achievable, since the Matlab function *pem()* uses standard numerical optimisation techniques. The Matlab function *lft()* was employed as well, but as seen in equation 3.2 in the method, the *lft()* command can simply be calculated by hand. Thus, the use of Matlab functions in this thesis should not be an issue when implementing the workflow in real life.

One crucial part of the workflow is that the estimations of transfer functions are fairly accurate with regard to the number of poles and zeros as well as the placement of these. Furthermore, it is important that the estimated system stays stable. If this is not the case, the estimation is probably wrong, since the system without controller is passive as discussed in section 5.2 and since the theoretically calculated transfer function is stable. Thus, comparisons of the poles and zeros as well as the step responses should be made between the theoretically calculated transfer functions and the estimated ones if it is possible.

It has also been discussed in length that the Matlab command *minreal()* was used

to cancel factors in the transfer functions with a specified tolerance. In reality a higher tolerance of distances between pole-zero pairs may be necessary to obtain the correct order of all transfer functions.

Regarding the notch filter, there are uncertainties that would make it difficult to get the exact frequencies of the resonances and as a result, it would be difficult to design this filter in reality. Furthermore, a resonant compensator would not be applicable in real life. However, it is of great interest to find a solution that would handle the resonances since it was not possible to get a stable transfer function from I_{adfsp} to I_{out} without filters.

6

Conclusions

The aim of this thesis was to find a workflow, based on control theory, to be applied to grid system identification and control of an electrical active dynamic filtering system. This thesis work was done under restrictions that simplified the environment to the extent that the result is not applicable directly in reality, but these methods set a foundation on how to work with more complicated, realistic environments.

Within the set limitations, this thesis has shown that it is possible to do system identification on a system consisting of the product from Comsys connected with an electrical grid which is either approximated as an L grid or an LCL grid. The system identification could be done using solely available data from the given measurement points. Furthermore, a method of tuning the PI controller parameters has been presented. Suggestions on how to incorporate additional filters in Comsys' product have been demonstrated as well.

Further investigations were also conducted into the use of I_{out} instead of I_{adf} when sending an error into the controller. Due to the significant oscillations between I_{out} and I_{adf}, this was deemed too challenging without applying some sort of resonance rejection filter to the system. Furthermore, using both I_{out} and I_{adf} was regarded as futile.

7

Future Work

As mentioned in the introduction, the goals of this thesis are the first initiatives in a larger project and naturally many future developments can be explored.

7.1 Eliminate Limitations in Thesis Scope

To make the result viable for a real-life product, the limitations discussed in section 5.5 and the limitations currently equipped to the problem formulations as of section 1.4, need to be taken into account. The real system handles three-phase AC power and thus, actions are required in implementing the result of this thesis, based on one phase power, onto the real product. When moving to the real-life system the occurrence of measurement noise and load disturbances can also be expected, which is not handled in depth in this thesis.

The continuous time nature of this thesis is not applicable to the actual product. The control analysis in this thesis was made on estimated continuous transfer functions and thus, the PI controller was also assumed to be continuous. The control system of the actual product is connected to a series of switches that produces the changes in voltage and current. These switches have a discrete time nature as well as the sampled measurements of the signals. The consequences that a change to discrete time would entail on the result, such as stability margins, have to be further investigated.

7.2 Control of Actual Output Signal

This thesis focuses on controlling the signal I_{adf} by feedback and sending the signal $I_{err} = I_{adfsp} - I_{adf}$ to the PI controller. This is seen as a step towards controlling the signal I_{out}, which is the actual current produced by the product. In the present situation I_{out} is not measured, but it is possible that it will be measurable in the future. This could enable adding control of that final signal, either by having it follow I_{adf} or I_{adfsp} directly. This thesis briefly examined the consequence of changing the

relevant output signal to I_{out} and it was concluded that the resonances made it more challenging to obtain a stable transfer function between I_{adf} and I_{out}. Thus, further investigations on filters to handle the resonances or other ways to control I_{out} will be needed in the future.

7.3 Investigate the Possibility of Practical Implementation

As mentioned above, the data used in this thesis was obtained from simulations in Simulink. Developments towards applications in real life would be to acquire data directly from the real product instead of a Simulink model. This would test the workflow on a more complicated and unknown grid to evaluate its adaptability as well. Another possible way would be to measure the grid when it is installed and tune the controller and filter at that time. However, this would not be a step in the direction of a fully automated system.

The research of this thesis has been exclusively conducted in Matlab. The availability of existing functions in the Matlab toolboxes has therefore benefited the work (as discussed in section 5.6). Examples of which are *pem()* and *lft()*, which have to be rewritten and implemented in a way that the script could be run on limited hardware and with as small time complexity as possible. Therefore, an investigation into what algorithms work best for the estimation of the transfer function must be conducted. This should be done by minimising the error with different numerical optimisation techniques.

Bibliography

Alfredsson, A. and R. Rajput (2009). *Elkretsteori*. Liber.

Åström, K. J. (2019). *Feedback fundamentals*. Automatic Control LTH, Lund University. URL: https://www.control.lth.se/fileadmin/control/staff/KJ/FeedbackFundamentals.pdf (visited on 2024-05-21).

Comsys AB, . (2024a). *Adf technology*. URL: https://comsys.se/power-quality-solutions/ (visited on 2024-04-08).

Comsys AB, . (2024b). *Our story*. URL: https://comsys.se/our-story/ (visited on 2024-03-26).

Ducard, G. (2018). *Signals and systems, lecture 10: filtering: applied concepts*. Institute for Dynamic Systems and Control, ETH Zurich. URL: https://ethz.ch/content/dam/ethz/special-interest/mavt/dynamic-systems-n-control/idsc-dam/Lectures/Signals-and-Systems/Lectures/Fall2018/Lecture10sigsys2018.pdf (visited on 2024-04-18).

Frazzoli, E. (2017). *Control systems i, lecture 12: loop shaping*. Institute for Dynamic Systems and Control, ETH Zurich. URL: https://ethz.ch/content/dam/ethz/special-interest/mavt/dynamic-systems-n-control/idsc-dam/Lectures/Control-Systems-1/Lectures/L1712-LoopShaping.pdf (visited on 2024-04-16).

Hägglund, T. (2009). *Lecture Notes Automatic Control*. Department of Automatic Control, Lund University, Faculty of Engineering, 221 00 Lund.

Henderson, M. I., D. Novosel, and M. L. Crow (2017). *Electric power grid, modernization trends, challenges, and opportunities*. URL: https://www.cmu.edu/epp/irle/readings/henderson-novosel-crow-electric-power-grid-modernization.pdf (visited on 2024-03-26).

Hespanha, J. (2009). *Linear Systems Theory*. Princeton University Press.

Linjengren, D. (2011). “Styrmetod och styrsystem för ett aktivt filter för resonansreduktion”. SE1151122 A1. Swedish Patent. URL: https://tc.prv.se/spd/patent?p1=PQz1MsebDIF7eM42P9NdVA&p2=8wxK9gjVlyY&content=Comsys&lang=en&tab=1&hits=true&range=10&hitsstart=10&start=11.

Ljung, L., T. Glad, and A. Hansson (2015). *Reglerteknik Grundläggande teori*. Studentlitteratur.

Ljung, L., T. Glad, and A. Hansson (2021). *Modeling and Identification of Dynamic Systems*. Studentlitteratur.

Montandon Neto, J. L. and T. B. Cunha (2019). *A brief survey of the gap metric for stability analysis*. Anais. São Carlos, SP: EESC-USP. URL: https://repositorio.usp.br/directbitstream/bf4813ad-d143-4598-8e28-7702868bcdb4/OK___trabalho%2007%20-%20A%20Brief%20Survey%20of%20the%20Gap%20Metric%20for%20Stability%20Analysis%20%28SIPGEM%202019%29.pdf (visited on 2024-05-21).

8

Appendix

8.1 Standard Grid Parameters

These are the parameters used in simulations if others are not stated. They are somewhat close to real-life parameters, but they do not represent the real-life system.

Low pass filter		
L1	2π·150e-6 H	Left inductor in low pass filter
L2	2π·50e-6 H	Right inductor in low pass filter
Cac	2π·50e-6 F	Capacitor in low pass filter
R	1e-3 Ω	All resistors in low pass filter
Grid		
Lg1	2π·100e-6 H	Right inductor in grid
Lg2	2π·50e-6 H	Left inductor in grid
Cg1	2π·50e-6 F	Capacitor in grid if LCL grid
Cg1	2π·50e-9 F	Capacitor in grid if L grid
R	1e-3 Ω	All resistors in grid
U_grid	10 V	Voltage in grid
base_freq	50 Hz	Base frequency
Controller		
Kp	1	Proportional term of controller
Ki	1000/π	Integral term of controller
Simulation		
fs	1e6 Hz	Sample frequency
T_simu	0.050 s	Simulated time

8.2 Simulink Model

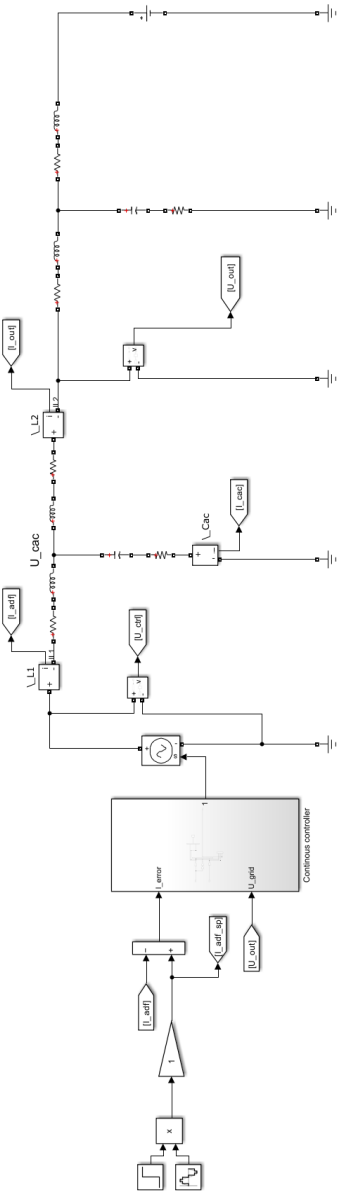

Figure 8.1 Simulink model.

Lund University
Department of Automatic Control
Box 118
SE-221 00 Lund Sweden

Document name
MASTER'S THESIS

Date of issue
June 2024

Document Number
TFRT-6234

Author(s)
Max Rosenbäck
Frida Salehi

Supervisor
Nils Lundström, Comsys AB, Sweden
Richard Pates, Dept. of Automatic Control, Lund University, Sweden
Anders Rantzer, Dept. of Automatic Control, Lund University, Sweden (examiner)

Title and subtitle
Control Analysis of Active Dynamic Filtering Systems for Electrical Power Application

Abstract

This thesis investigates the behaviour of an active dynamic filtering (ADF) system connected to an unknown electrical grid and suggests how to use control theory to reach desired requirements. The ADF system, which is based on a product by Comsys AB, consists of a PI controller and a low pass filter.
The main part of this work was focused on developing methods for system identification by finding transfer functions between available signals utilising a grey box model approach. Different validation techniques were applied to gain trust in the model as well as the estimated transfer functions. By reworking the model and by using the estimated transfer functions, the electrical circuit could be reformulated as a block diagram to facilitate the use of standard control analysis. Methods of tuning the PI controller parameters to reach a certain bandwidth while keeping stable margins were presented. It was concluded that the resonances in the open loop transfer function had to be counteracted. Therefore, filter designs to compensate for this behaviour were also investigated and presented. Finally, a number of future developments were presented.
In conclusion, the method of estimating the transfer functions, yielding the system identification, is shown to be sufficient. Thus, the system behaviour can be understood and can be altered to achieve different requirements through control parameter tuning and filters. Future research could expand this work by applying this workflow on more realistic systems.

Keywords
System identification, PI controller, Electrical grid, Notch filter, Automatic control, Grey Box, Simulink

Classification system and/or index terms (if any)

Supplementary bibliographical information

ISSN and key title
0280-5316

ISBN

Language
English

Number of pages
1-74

Recipient's notes

Security classification

http://www.control.lth.se/publications/